INTERNATIONAL ATOMIC ENERGY AGENCY
UNITED NATIONS EDUCATIONAL, SCIENTIFIC AND CULTURAL ORGANIZATION

INTERNATIONAL CENTRE FOR THEORETICAL PHYSICS
34100 TRIESTE (ITALY) - P.O.B. 586 - MIRAMARE - STRADA COSTIERA 11 - TELEPHONE: 2240-1
CABLE: CENTRATOM - TELEX 460392-I

H4.SMR/222 - 11

SECOND AUTUMN WORKSHOP ON CLOUD PHYSICS AND CLIMATE

(23 November - 18 December 1987)

REMOTE SENSING, SATELLITE AND RADAR METEOROLOGY

G. Dugdale
Dept. of Meteorology
University of Reading
U.K.

CONTENTS

SYLLABUS

This course examines the methods of observing the atmosphere and the earth's surface by satellite born radiometers and by radar from surface and space platforms. The spectral variation of the absorption, scattering the emission of electromagnetic radiation by the various constituents of the atmosphere allows deductions to be made about the distribution and temperature of the gases. The temperature of the earth's surface can be measured from satellites by monitoring its thermal emission in the frequency bands in which the atmosphere is relatively transparent. Rainfall rates can be estimated from the reflectivity of precipitating clouds in the micro-wave region. Wind velocity can be measured by tracking clouds and rainfall estimates can also be made from the association of rain with satellite observed cloud characteristics.

The physical properties of the atmosphere which allow these measurements and which limit their accuracy are considered. The platforms, instrumentation and data treatment techniques are described.

Electromagnetic radiation and the atmosphere

Atmospheric absorption and emission: black body emission, width and shape of spectral lines and bands, the atmospheric absorption spectrum.
Radiation transfer: Schwatzchild's equation, transfer in a plane parallel atmosphere, the diffusive approximation, atmospheric transmission models, weighting functions.
Scattering and refraction of radiation: Rayleigh and Mie scattering, scattering by non-spherical particles and populations of particles, refraction in a plane parallel atmosphere.

Satellite meteorology

Satellites: types, orbits, types of radiometers, scanning techniques.
Soundings of the earth's surface: visible, near IR, IR and microwave soundings for surface reflection characteristics, surface temperature and moisture, the atmospheric corrections.
Soundings of the atmosphere: retrieval of temperature and humidity profiles, radiometers, soundings for trace gases, limb scanning, cloud imagery and wind finding, rainfall estimation.

Radar meteorology

Atmospheric effects: refraction, absorption and scattering of microwave radiation by the atmosphere and its constituents.

Radar: the radar equation, doppler radar, polarized beams.

Measurements: rainfall estimation, radar for research, active microwave sensing from satellites.

Texts

Radar observation of the atmosphere - L.J. Batten (Chicago Univ. Press)

Remote sensing in Meteorology, Oceanography and Hydrology, ed. A.P. Cracknell (Ellis Horwood) ch. 1, 24, 25.

Radiative processes in Meteorology and Climatology - Paltridge and Platt (Elsevier).

Remote sounding of atmospheres - Haughton, Taylor & Rodgers (Cambridge Univ. Press).

1 - INTRODUCTION

What is Remote sensing:- the measurement or detection of a physical property from a distance. Usually by the characteristic emission or scattering of E - M radiation or sound waves.

Why Remote sensing:- convenience, cost, accuracy.

Applications 1) Routine Meteorological: replacement of or supplementary to meteorological network data.
e.g. Sea surface temperature, winds over the oceans and atmospheric soundings.
In these cases area mean values over scales of tens or hundreds of km are needed with accuracies similar to those specified for synoptic observations.
(See Table 1).
A mixture of orbitting and geostationary satellites can give the spatial and time resolution but absolute accuracy of most quantities is less than the requirement. However, it is probably better than much conventional synoptic data which while precise does not usually give a good average over space or time so is influenced by sub synoptic scale events and local effects.

2) Hydrological: snow cover, precipation and lake area measurement. Observations over specified catchment areas on scales of km or tens of km.

3) Research & Special applications: Radiation balance, measurement of minor atmospheric constituents, sea state, surface topography, crop monitoring, pest control etc.

Table 1

The Global Atmospheric Research Programme of WMO recommended accuracies for atmospheric soundings.

Quantity	Accuracy (r.m.s. error)
Wind component	$\pm$ 3 m s $^{-1}$
Temperature	$\pm$ 1 K
Water vapour pressure	$\pm$ 1 mb
Sea surface temperature	$\pm$ 0.2 K
Pressure reference level	$\pm$ 0.3%

Data required on a 100 km grid, at eight standard levels in the atmosphere

(Surface 900, 700, 500, 200, 100, 50 and 20 mb), twice per day.

General types of sensor system

Fig. 1.1

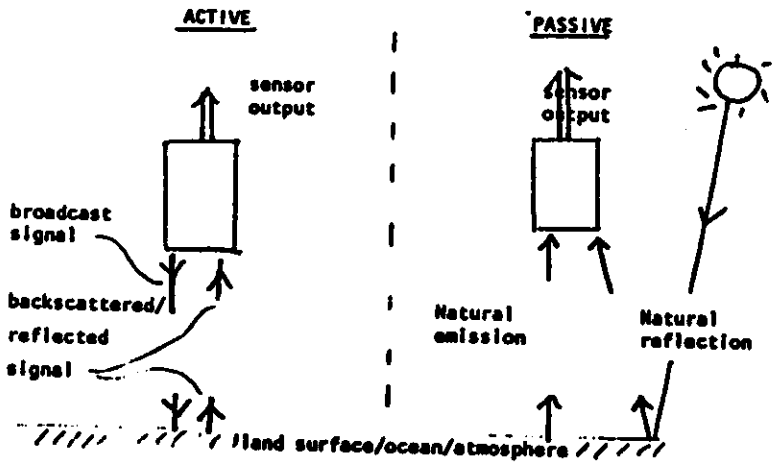

- Passive sensors: passively measure/interpret signal information coming directly from the field of observation. e.g. radiation thermometer.
- Active sensors: transmit a signal towards the field of observation and measure the reflected return signal. e.g. weather radar.

Sensor output may be,

(i) analogue in which the sensor output is a continuous function of the input signal - e.g. the record of a chart recorder connected directly to a solarimeter (pyranometer), or

(ii) digital - the input signal is sampled in space and/or time and digitally coded as a data stream. Such signals are most easily handled by communications and computing systems so most analogue outputs are digitsed before transmission.

The Remote Sensing Problem

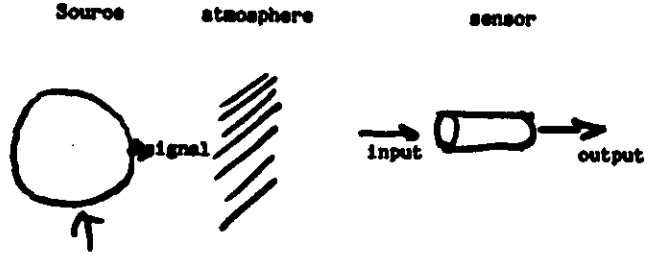

(i) The signal from the source may not be a function only of the quantity it is intended to measure.

(ii) Absorption, emission and scattering by the intervening atmosphere may cause the input signal to differ from the source signal and the difference almost certainly will depend both on the source signal and the state of the atmosphere.

(iii) The sensor calibration will vary with temperature and other variations so frequent calibration may be necessary.

In practice it is usual to have some local measurements made (ground truth) against which the remotely sensed data can be compared. For most purposes a mixture of measuring techniques using perhaps several remote sensing systems together with some "ground truth" is the most satisfactory.

The Electromagnetic Spectrum

Most remote sensing techniques depend on the relation between the quantity to be sensed and E - M radiation. Radiation in the wavelength range 0.01 μm to 50 cm are useful in remote sensing.

The E - M spectrum

Fig.1.2

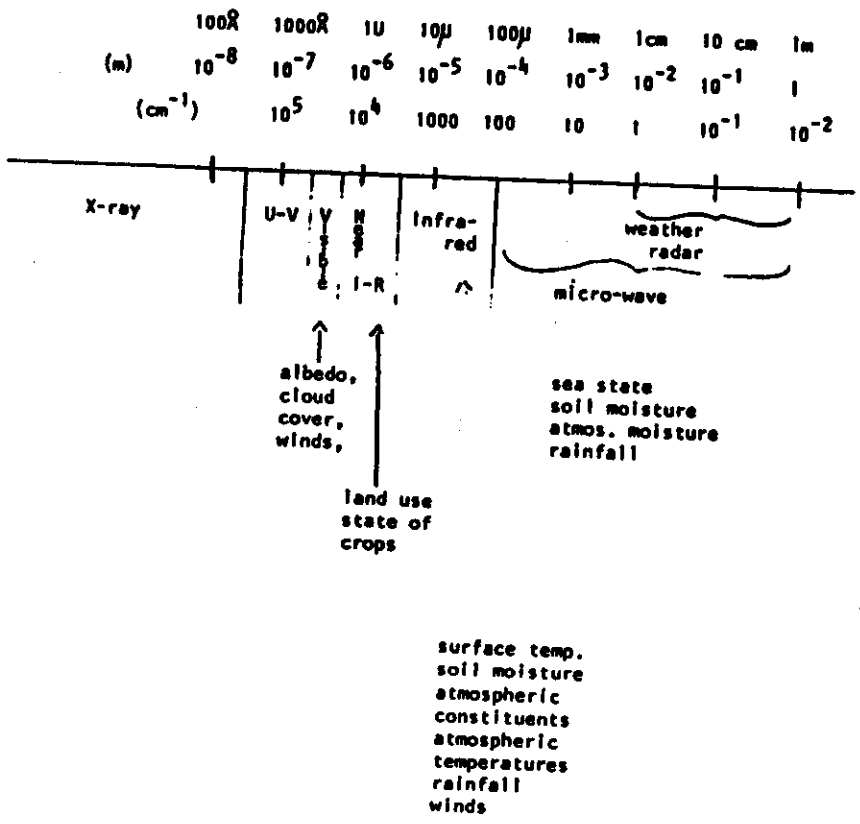

2 - RADIATION AND THE ATMOSPHERE ABSORPTION AND EMISSION

References

Radiation Notes (RPP) Paltridge & Platt, Haughton.

2.1. Energy of a molecule

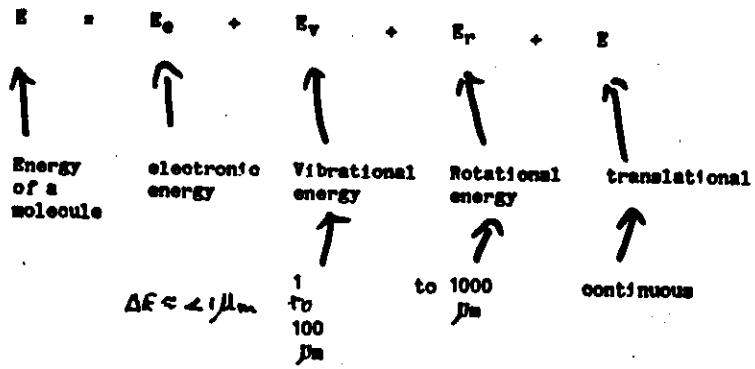

2.2. Local thermodynamic equilibrium (L.T.E.)

When molecules interact, "collide", their energy is redistributed among the components.

The emission of energy when changing state takes a finite time say ϕ, if the time between collisions $\gamma \ll \phi$ any absorbed energy will be redistributed before re-emission. If $\phi \ll \gamma$ there will be re-emission at the same frequency.

In the lower atmosphere $\gamma \ll \phi$ so we have L.T.E.

At L.T.E. atmospheric gases absorb and emit radiation at frequencies corresponding to changes in vibrational and rotational energy levels.

Except for consideration of O_3 high in the atmosphere we shall assume L.T.E.

2.3 Shape of absorption "lines"

a) Intrinsic width - if energy states were precisely defined energy absorption and the frequency of emission would be determined by $\Delta E \approx h\nu$

However, we cannot determine both β and E for any energy level precisely (Heisenburg) $\therefore$ there is uncertainty in ΔE and in the associated ν or λ

This width of line is insignificant for rotational or vibrational changes.

b) Doppler broadening

As the molecules will be moving away from or towards the observer while emitting this gives a Doppler shift.

$$\Delta\lambda = \lambda_0 \frac{v}{c}$$

v is the component of vel. along the line of sight.

c is the speed of light.

Within a population

$$n(\nu_0 \pm \delta\nu) = e^{-(\delta\nu)^2}$$

(Gaussian)

This gives a shape

$$k_\nu = \frac{S}{\alpha_D \pi^{1/2}} \exp\left[-\left(\frac{\nu-\nu_0}{\alpha_D}\right)^2\right] \quad \text{with } \alpha_D = \frac{\nu_0}{c}\left[\frac{2RT}{M_r}\right]^{1/2}$$

where k_ν is the absorptivity at ν

S is the line strength

α_D is the doppler half width

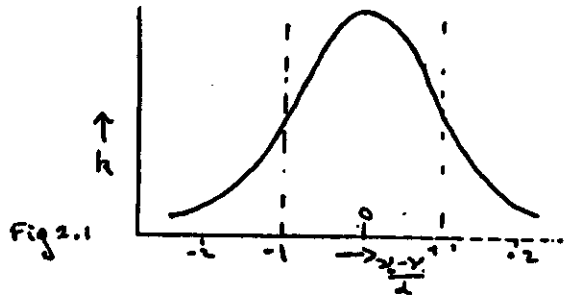

Fig 2.1

Doppler broadening is important only in the high atmosphere.

c) Pressure broadening

Interactions between molecules in close proximity cause changes in the energy levels, thence change the frequency of emissions between levels. So the broadening is related to the frequency of "collisions" between molecules.

α_L is the Lorents half width

and $k_\nu = \frac{S\alpha_L}{\pi[(\nu_0-\nu)^2+\alpha_L^2]}$

In the atmosphere changes of p are generally large c.f. changes in T $\therefore \alpha_{Lp} \approx \alpha_{L_0} \frac{p}{p_0}$

If we wish to make calculations in the atmosphere $\bar{p}$ will, in general, not be constant along the path. In this case we adopt the "Curtis - Godson" approximation

$$\bar{p} = \frac{\int p \rho_a \, dz}{\int \rho_a \, dz}$$

where ρ_a is the local density of absorber along the path S.

Note for atmospheric calculations we often use $\rho_a = c\rho_{at}$ where ρ_{at} is the total atmospheric density and c the mass fraction of absorber.

2.4 Integrated absorptance of a line (W)

This is the total effect of absorption by a line along a defined atmospheric path.

Transmission over $\tau = \exp -(k_\nu \rho l)$

where ρ is the density of absorber in a path l

$$W = \int_{-\infty}^{\infty} (1 - \tau_\nu)\, d\nu$$

N.B. If $k_\nu \rho l$ is small

$W = S \rho l$ (This is true for any shape of line)

If $k_\nu \rho l$ is large, $\tau \to 0$ near the line centre

and $k_\nu = \frac{S \alpha_L}{\pi (\nu_0 - \nu)^2}$ for a pressure broadened line away from the centre.

giving $W = 2 (S \alpha_L \rho l)^{1/2}$

Fig 2.2

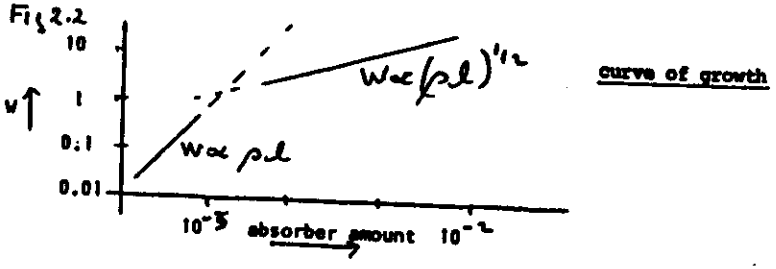

curve of growth

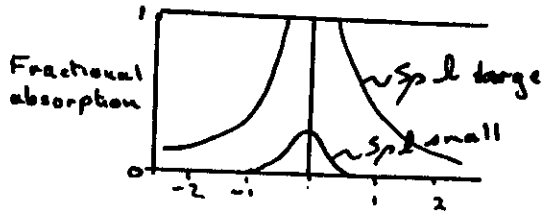

2.5 Absorption bands

Absorption in the atmosphere is generally in bands which are composed of a number of closely spaced "lines" (see diagrams overleaf).

a) Elsasser model - an infinite array of equally spaced, of equal S and equal α_L the half width of Lorenty shaped lines.

$$k_\nu = \sum_{i=-\infty}^{i=+\infty} \frac{S}{\pi} \left(\frac{\alpha_L}{(\nu_0 - \nu + i\delta)^2 + \alpha_L^2} \right)$$

where δ is the space between the lines.

For small S gives the exponential decrease in transmission with path length.

For large S gives an error function decrease $\left[ERF(x) = \frac{2}{\pi} \int_0^x e^{-\theta} d\theta \right]$

$$\tau = 1 - ERF(\pi \rho l S \alpha_L)$$

This model is a reasonable representation of the 15 Um CO_2 bend.

b) Goody model an infinte array of randomly spaced lines having the same half width and strengths S according to

$$\text{Prob}(S) = \frac{1}{S_0} \exp -\left(\frac{S}{S_0}\right)$$

where S_0 is the mean line strength

Solves to

$$\tau = \exp -\left[\frac{S_0 \rho l}{\delta \left(1 + \frac{S_0 \rho l}{\pi \alpha_L}\right)^{\frac{1}{2}}} \right]$$

if $\frac{S_0 \rho l}{\pi \alpha_L}$ is large

$$\tau = \exp -\left[\frac{S_0 \rho l \pi \alpha_L}{\delta} \right]$$

Can be applied to W.V. rotation/vibrational bands using values for S_0, α_L and δ derived from quantum mechanics or experiments.

Fig 2.4

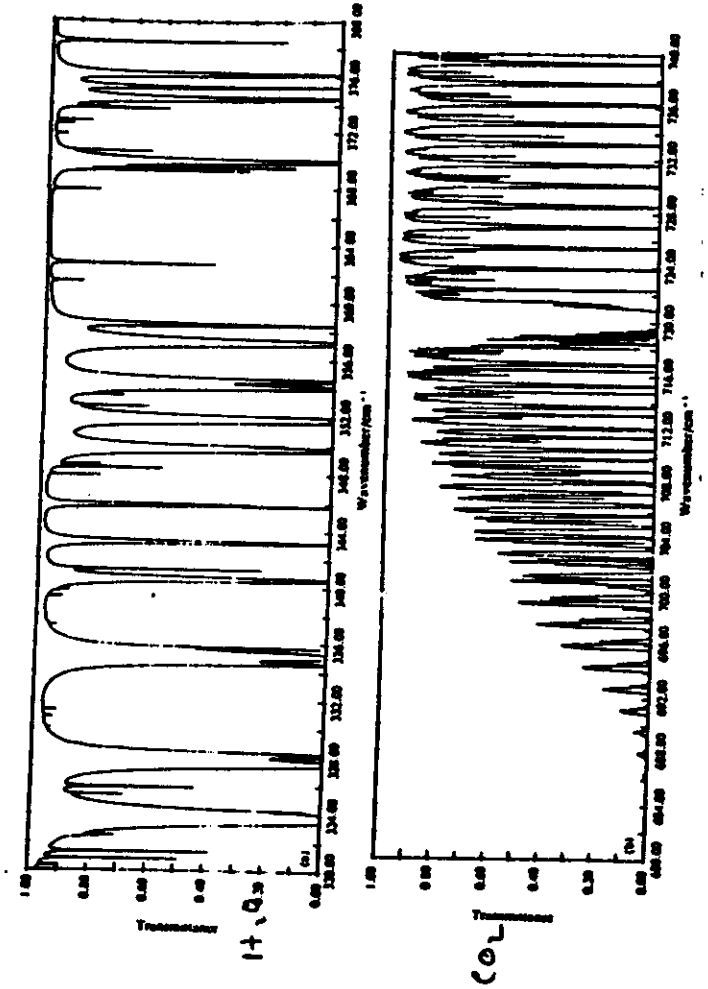

FIGURE 2.5

Atmospheric absorptions (and emissions)

after Goody, R.M., *Atmospheric Radiation*, p.4

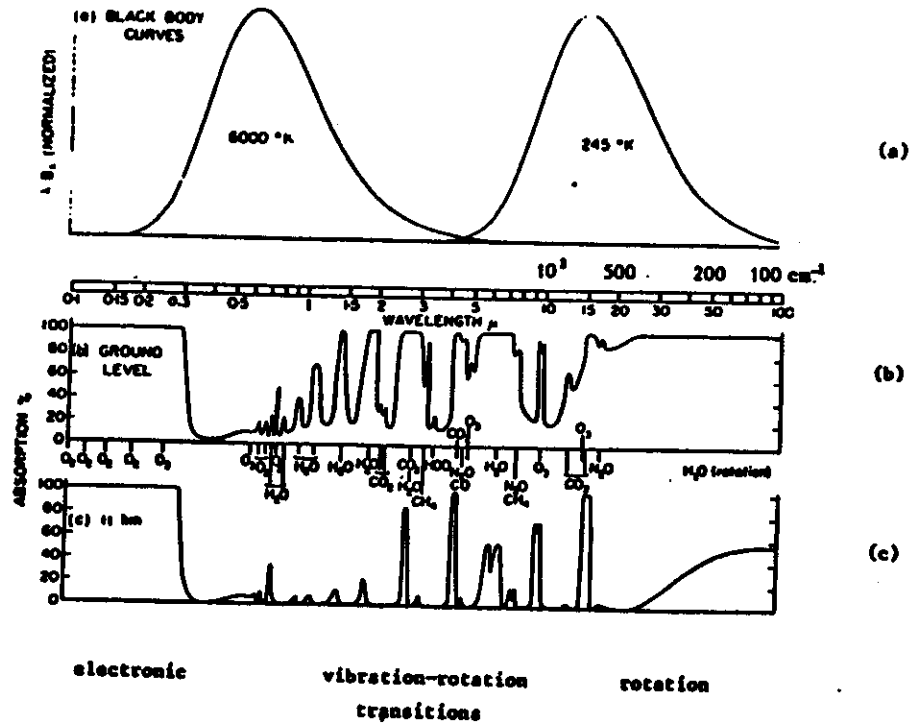

(a) Blank-body curves for 6000° K and 245° K. (b) Atmospheric gaseous absorption spectrum for a solar beam reaching ground level. (c) The same for a beam reaching the temperate tropopause. The axes are chosen so that areas in (a) are proportional to radiant energy. Integrated over the earth's surface and over all solid angles the solar and terrestrial fluxes are equal; consequently, the two black-body curves are drawn with equal areas beneath them. An absorption continuum has been drawn beneath bands in (b). This is partly hypothetical because it is difficult to distinguish from the scattering continuum, particularly in the visible and near infra-red spectrum. Conditions are typical of mid-latitudes and for a solar elevation of 40° or diffuse terrestrial radiation.

2.6 Black body emission

a) Total emission

M_B or $B = \sigma T^4$ Stefans const. $\sigma = \frac{2\pi^5 k^4}{15 c^2 h^3}$ Boltzmann, Planck

b) Spectral distribution

$$B_\lambda = \frac{c_1}{\lambda^5}\left(\frac{1}{\exp\left(\frac{c_2}{\lambda T}\right)-1}\right)$$

$c_1 = 2\pi h c^2 = 3.74 \times 10^{-16}$ W m^{-2}

$c_2 = \frac{hc}{k} = 1.439 \times 10^{-2}$ m deg K

diff to give $\lambda_{max} T = 2.897 \times 10^{-3}$ m deg K.

c) Grey body - one which emits isotropically with an emissivity constant at all wavelengths

Fig 2.6

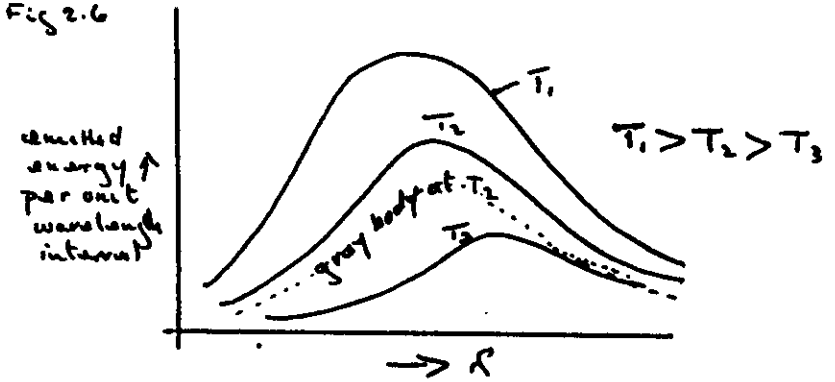

2.7 Monochromatic transmission through a horizontally stratified atmosphere

Fig 2.7

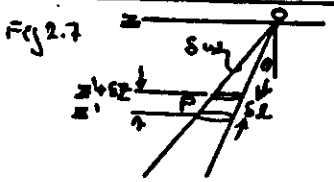

Consider the flux through a horizontal area at 0 originating in the layer at P occupying a solid angle $\delta\omega$ at an angle θ to the vertical.

Monochromatic radiance from P towards 0

$$= k_\nu \rho_\nu \delta l \, N_B(\nu,T)$$

$$= k_\nu \rho_\nu \delta z \sec\theta \, N_B(\nu,T)$$

Transmission between P and 0

$$= \exp -\int_{z'}^{z} \rho k \sec\theta \, dz$$

omitting monochromatic subscripts

2.7 cont.

The diffusive approximation

The integral in eq. 2 is a third order exponential integral the solutions to which have for all practical purposes the same shape as

$$\exp -\int_{z'}^{z} \beta\rho k \, dz = 2\int_0^{\pi/2} \text{etc} \, d\theta = \tau(z,z')$$

with $\beta = 5/3$

So for diffuse radiation we use a model of direct beam transfer and apply the appropriate form of Beer's law and Schwartzchilds eq.

2.7 The diffusive approximation makes clearer the weighting function $\delta\tau$

z ——————

$z+\delta z$ ——————

z' ——————

—— layer δz absorptivity $(\rho \delta z k)$ for a parallel beam or $(\rho \delta z k/\beta)$ for diffuse radiation

——————

Contribution of slab to flux at z, ΔF

$$\Delta F = \rho \delta z \beta k N_B \tau(z+\delta z, z)$$

Transmissivity of layer z $\exp -\bar{\rho} \delta z \beta k \approx 1 - \rho \delta z \beta k$

Transmissivity z' to z $= \tau(z',z) = \tau(z'+\delta z, z) \cdot \tau(z', z+\delta z)$

$$= \tau(z'+\delta z, z)(1 - \rho \delta z \beta k)$$

$$\therefore \frac{\partial \tau}{\partial z} = \frac{\tau(z'+\delta z, z) - \tau(z',z)}{\delta z} = \tau(z'+\delta z, z)\rho\beta k$$

or

$$\Delta F = N_B \delta\tau$$

Note the above is equally applicable to a directional radiometer viewing through a stratified atmosphere. In this case β is omitted from the equations and, if viewing is at an angle θ to the vertical at term $\sec\theta$ is included in the absorption and transmission terms.

2.8 Weighting functions

For a radiometer viewing vertically downwards the received radiance

$$N_\nu = \underbrace{\int_0^\infty B_\nu \frac{\partial \tau}{\partial z} dz}_{\text{sky}} + \underbrace{B_{\nu s}(T_s)\,\tau_\nu(0,\infty)}_{\text{ground}} \qquad N_\nu = B$$

It is convenient computationally to use a vertical scale in y, $y = -\ln \frac{p}{p_0}$, $dy = -\frac{1}{p}dp$

$$N_\nu = \int_0^\infty B_\nu K(y)\, dy + B_{\nu s}\tau(0,\infty)$$

where $K(y)$ is the weighting function in terms of y.

Notes: (i) Sym. Sz (mean isothermal atmosphere); (ii) $p_0 = 1$

e.g. a) An absorber with k_ν independent of p and T

$$\tau_{y,\infty} = \exp - \int_p^0 k_\nu \frac{r}{g} dp \quad \text{where r is the mass mixing ratio at p}$$

$$= \exp - k_\nu \frac{r p}{g} \quad \text{for r constant}$$

$$K_y = \frac{\partial \tau(y,\infty)}{\partial y} = -p \frac{\partial \tau(y,\infty)}{\partial p}$$

$$= \frac{p k_\nu r}{g} \exp - \left(\frac{k_\nu r p}{g}\right)$$

Max. when $\frac{\partial K}{\partial p} = 0$

i.e. when $\frac{k_\nu r}{g} = \frac{1}{p}$ or when $p \frac{k_\nu r}{g} = 1$

i.e. Unit optical depth from the top of the atmosphere.

b) Weighting function in the wing of a pressure broadened line

$$k_\nu = \frac{S d_L}{\pi\left((\nu_0 - \nu)^2 + d_L^2\right)}$$

$$\approx \frac{S d_L}{\pi (\nu_0 - \nu)^2} \quad \text{when } |\nu_0 - \nu| \gg d_L$$

$$\therefore \tau_{(y,\infty)} = \exp - \int_p^0 \frac{S d_L}{\pi (\nu_0 - \nu)^2} \cdot \frac{r}{g} dp$$

where d_L is given by $d_L = d_{L_0} \frac{p}{p_0}$

$$K_y = \frac{\partial \tau}{\partial y} = -p \frac{\partial \tau}{\partial p} = A p^2 \exp\left(-\frac{A p^2}{2}\right) \quad \text{with r independent of p}$$

and $A = \frac{S d_{L_0} r}{\pi (\nu_0 - \nu)^2 p_0}$

$K(y)$ is a maximum when $\frac{\partial K}{\partial p} = 0$

$$2p = A p^3 \quad \text{or} \quad p_m = \sqrt{2/A}\,; \quad A = \frac{2}{p_m^2}$$

$$K_y = 2\left(\frac{p}{p_m}\right)^2 \exp\left(-\frac{p}{p_m}\right)^2$$

with $p_m^2 = 2\pi g p_0 \frac{(\nu_0 - \nu)^2}{S d_{L_0} r}$

It is usual to define the pressure in atmospheres so $p_0 = 1$

c) The Elsasser band

$$\tau = 1 - \frac{2}{\pi} \int_{B\rho}^{\infty} \exp(-x^2)\, dx$$

B depends on S, d_L, δ, and r

a complex integration problem results in

$$K(y) = \left(\frac{2}{\pi}\right)^{1/2} \frac{p}{p_m} \exp\left(\frac{-p^2}{2 p_m}\right)^2$$

3 - SOME CHARACTERISTICS OF SATELLITES AND OF RADIOMETERS

General reference

Climatology from Satellites - Barrett.

3.1 The main types of environmental sensing satellites.

a) Polar orbiting meteorological satellites.

These satellites orbit the earth at about 1000 km altitude which gives a period (T) of about 100 minutes. The plane of orbit is tilted slightly from the earth's axis and is fixed relative to the sun-earth line. This ensures that on each orbit the satellite crosses any line of latitude at a fixed solar time and views the daylight and night side of the earth once each orbit.

The width of the swath scanned by the radiometers on each orbit must be at least 25° at the earth's surface in order that consecutive swaths should overlap and give global coverage twice each day; once in daylight and once at night.

b) Geostationary meteorological satellites.

These satellites orbit the earth at about 36,000 km altitude which gives a twentyfour hour period of rotation. The orbit is in the plane of the earth's equator and the direction of rotation is the same as that of the earth. Hence the satellite remains stationary relative to the earth and can be positioned over any preselected point on the equator.

The high altitude of such satellites limits the spatial resolution with which the earth can be viewed. However, because they are geostationary frequent images of the same area can be obtained. Typically forty-eight images per day are taken.

The earth is scanned by the rotation of the satellite about its axis which is parallel to the earth's axis. The width of the scan line on the earth's surface is from one to five kilometers at the satellite sub point. A stepped motor changes the latitude of the scan line each rotation of the satellite to build up the complete image of the earth.

c) Earth resources satellites - a series of experimental and operational satellites of which LANDSAT is the best known. The altitude and orbits are similar to the orbiting meteorological satellites but the radiometers carried have a much narrower field of view. This gives a ground resolution of a few tens of metres but restricts the area covered to a narrow strip beneath the orbit so that it takes about eighteen days to build up a complete global image.

So we see that there has always a compromise to be made between spatial and temporal resolutions. The type of satellite to be used to study any particular phenomenon depends on the size and time scale of that phenomenon.

3.2 Some properties of satellite instrumentation

a) The detectors

Early satellites often used television type "cameras" to view the earth. These have been replaced almost entirely by radiometers which scan a narrow strip of the earth, the output from which is sampled to give the required resolution along the strip. The scan may be achieved by the rotation of the satellite or by swinging the radiometer or its optical system. The former method is used for geostationary satellites and was used in the early polar orbiting satellites. Later orbiters are controlled so that the instrument console always points towards the earth and the radiometers scan perpendicular to the satellites path across the earth.

Radiometers may observe the electromagnetic radiation reflected or emitted from the surface below over a wide range of frequencies. These may include several bands in the visible and near infra red, one or more bands in the termal infra-red and micro-wave bands. The uses of the different bands will be discussed in later sections of this paper.

b) Spatial resolution

The spatial resolution of a radiometer is limited by the diffraction limit and by the signal to noise ratio.

The diffraction limit is imposed by the size of the aperture or objective of the radiometer and may be expressed as $\alpha = 1.22 \lambda / D$ when λ is the wavelength of the radiation, D the aperture diameter and α the maximum angular resolution.

The spatial resolution is also limited by the energy available from the source area within the waveband being observed. If this energy is too low the signal will be masked by the noise generated within the radiometer and its associated electronic circuits.

c) Wavelength resolution

For many purposes the information which can be deduced from radiometric data depends on how narrow a waveband can be observed. Again, the narrower the waveband the lower the signal to noise radio so this eventually limits the resolution. Also the characteristics of the filters used to define the waveband introduce limits on how narrow the band can be.

d) Sensitivity of a radiometer system

The sensitivity of the radiometer depends on several factors including the characteristics of the optics and filters, the detectors and the amplifiers. This is illustrated overleaf.

Fig 3.1

Filters

Filter transmission

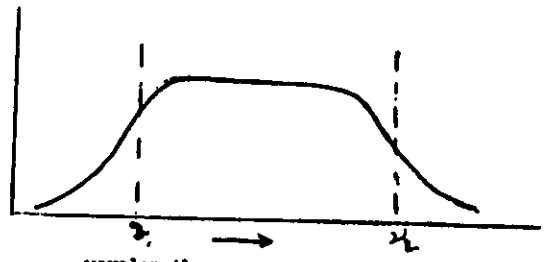

Detectors (photo electric or thermo-electric)

Detector output for a signal of constant energy per unit spectral interval

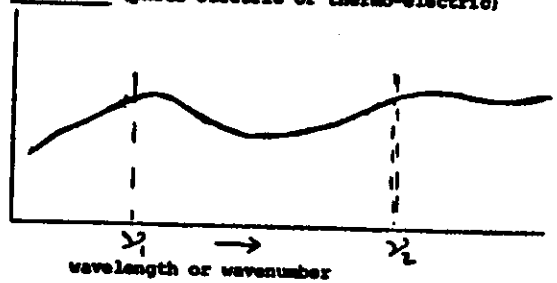

Amplifiers and electronics

Amplification

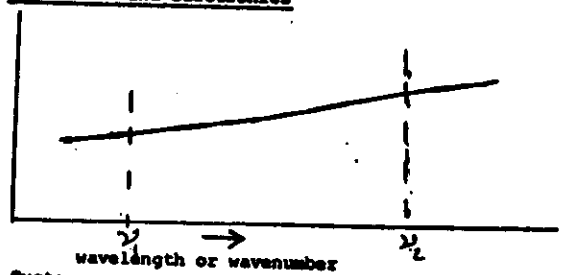

System response

System response (S_ν)

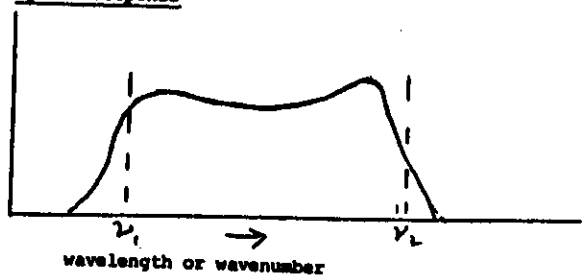

The output of the radiometer is given by $\int_\nu N_\nu S_\nu \, d\nu$

where N_ν is the input radiance

4 - ATMOSPHERIC SOUNDINGS

(Main reference, Remote sounding of the Atmosphere, Haughton, Taylor and Rogers).

Given the surface temperature, the vertical distribution of the atmospheric temperature and of atmospheric absorbers and scatterers and their absorption scattering properties, we can calculate the radiance which would be received by a radiometer viewing the earth from space. The question we address in this section is "to what extent can we deduce the vertical distribution of atmospheric temperature and atmospheric constituents from the readings of radiometers in space?" The problem of scattering will be mainly left aside.

The interpretation of the radiometer signal is clearly simpler if we choose a waveband or wavebands in which only a single absorber is present. In this case the outgoing radiance has two components, the attenuated signal from the earth's surface and the radiation originating in the atmosphere. For most purposes we choose wavebands which absorb strongly enough for the atmospheric signal to dominate strongly. Then, we can interpret the signal as the integral from the surface to space of the produce of the local temperature and the weighting function, assuming local thermodynamic equilibrium.

Even with the above simplifications there is still no unique interpretation of the integral in terms of either temperature or absorber concentration even though one of them may be known. For any temperature profile there are an infinite number of absorber concentration distributions which would give the same outgoing radiance and similarly for a defined absorber distribution there are an infinite number of temperature profiles which could give any specified outgoing radiance. While no unique solution can be found we can obtain good approximations by using a series of wavebands each having a sharply peaked weighting function.

4.1 Atmospheric temperature soundings

4.1.1. Selecting the waveband

The vertical monochromatic radiance outside the atmosphere (N_ϵ) may be written as:

$$N_\epsilon = \epsilon N_{sa} \tau_{(1,a)} + \int_1^a N_{Bp} \frac{\partial \tau}{\partial p} \delta p$$

where we are using pressure in atmospheres as the vertical co-ordinate. If we have a uniformly mixed absorber of known absorption properties we can calculate the weighting function. The more peaked the function the more information we have from each radiometer channel. Here compromises must be made between narrow wavebands which give strongly peaked weighting functions and broader bands which give more energy so larger signal to noise ratios. Figure 4.1 shows a typical set of weighting functions used by temperature sounding radiometers.

Figure 4.1

Weighting functions (gradient of transmission with respect to log pressure) for instruments sounding the temperature of the lower atmosphere on the Nimbus 6 satellite: (*a*) 15 μm channels of HIRS. (*b*) 4.3 μm channels of HIRS, (*c*) channels of SCAMS (c.f. § 6.9; from Smith and Woolf 1976 and Staelin *et al.* 1975).

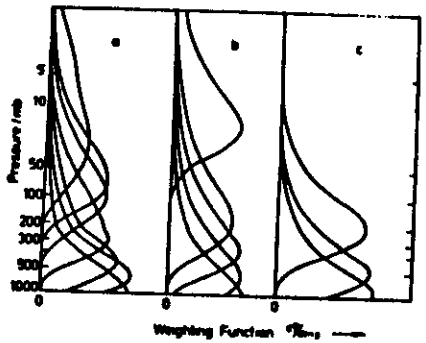

In deciding which wavebands should be used various criteria have to be met, namely:

a) the emitting gas should be uniformly mixed (CO_2, O_2),
b) the absorption band should not overlap the bands of other absorbing gases,
c) the bands should not overlap the solar spectrum,
d) local thermodynamic equilibrium (LTE) should prevail so that the Bolzman distribution of emission can be assumed,
e) the band should not be affected by the presence of cloud.

These properties of the CO_2 and O_2 bands are summarised below.

Band	LTE to	Sensitivity	Energy	Spatial resolution	Overlap	Influence of clouds
CO_2 4.2μm	35km	4% K^{-1}	good	good	solar	yes
CO_2 15μm	80km	1% K^{-1}	good	good	OK	yes
O_2 5mm	100km	1/3% K^{-1}	poor	poor	OK	little

Most operational temperature profile measuring schemes use the CO_2 15μm band and take measurements at a series of frequencies on the edge of the band. The measurements are not monochromatic but span a narrow band each wide enough to give a good signal to noise ratio. The emission comes from the sum of the emission from the wings of many lines. For the wing of a mono-chromatic Elasser band the weighting function K(y) is

$$K(y) = \sqrt{\frac{2}{\pi}}\left(\frac{p}{p_w}\right)\exp - \left(\frac{p}{p_w}\right)^2$$

The effect of using a narrow band is to broaden the weighting function.

4.1.2. Retrieval of temperature profiles from radiances

We wish to derive an atmospheric temperature profile from a series of measured radiances in wavebands on the edge of the absorption band of a uniformly mixed atmospheric gas.

4.1.2.1. The "exact" solution

Here we represent the temperature profile by a mathematical function which may for instance be a fourier series or a polynomial.

e.g. $T(z) = a + bz + cz^2$ etc.

Now

$$N_{b(\Delta\nu)} = \frac{1}{2\delta\nu}\int_{\nu-\delta\nu}^{\nu+\delta\nu} N_{B\nu}\, d\nu$$

$N_{b(\Delta\nu)}$: Black body radiance per unit spectral interval in the radiometer band

$N_{B\nu}$: monochromatic Planck f'n at (T_z)

K, the weighting function is known so we can express the received radiance in terms of the coefficients a, b, c etc and solve for as many coefficients as there are radiometer channels. The problem is that any errors in the measured radiances are amplified in terms of the derived temperatures. This effect is illustrated below.

Fig. 4.2

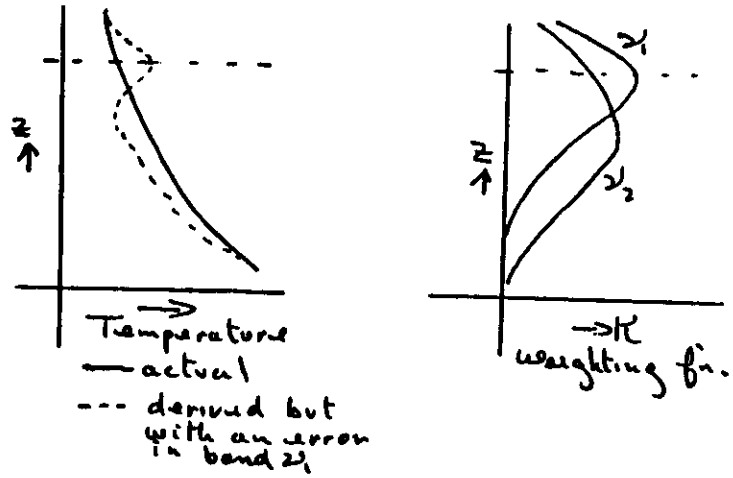

The closer the peaks of the weighting functions the greater the error in the spurious detail.

The effect may be minimised by choosing the most appropriate form of representing the temperature profile. This turns out to be a linear combination of the weighting functions themselves.

$T(z) = a K_{\nu_1}(z) + b K_{\nu_2}(z) + K_{\nu_3}(z)$ + etc

with N band = $\int_{band}\left[\int N_{B\nu} K_{\nu}\, dz\right] d\nu$

However temperature errors of up to 15 times the errors in measured radiances still occur.

4.1.2.2. Non-exact solutions

The above techniques may be modified to allow the derived temperature profile to differ from the exact solution by an amount corresponding to the known probable error in the radiance measurements.

Least squares approximate solutions

These involve defining the minimum number of coefficients which will give a temperature profile of the required precision then using many more measurements than coefficients and selecting the temperature profile which gives the best least squares fit. In practice, because we have only a few independant weighting functions these methods are difficult to apply. Bogus measurements may be introduced together with their expected errors (or variances). Such "measurements" may be derived from climatology or interpolations between radiosonde data. Spurious (and perhaps actual) detail may be removed from the derived profile by smoothing techniques which are related to the calculated maximum vertical resolution which could be expected from the data.

Iterative techniques

A first guess profile, which may itself be a mathematical or climatological profile, is adjusted to fit the observed data taking one radiometer band at a time and re-iterating until the solution converges. This eventually produces the same solution as the exact one but may be stopped before large spurious detail develops.

Regression techniques based on empirical data

Within a season or climatic zone it may be possible to establish relationships between the various combinations of radiometer band data and the temperature profiles as observed by radio-sounders. No knowledge of the weighting functions nor of the radiometer calibrations are needed. Such methods have to be "calibrated" for localised climatic and seasonal zones. They cannot pick out the unusual temperature distribution. Such methods are widely used operationally and dispense with the physics except in the design stage of the radiometers and in determining the height and temperature resolution which can be attained and which should be represented by the regressions.

4.1.3. Middle and upper atmospheric temperature sounding

At high altitudes LTE may not pertain also doppler broadening may become as important or more important than pressure broadening. Weighting functions must be calculated accordingly. Otherwise the vertical sounding techniques described above can be applied at high altitudes. However, at these levels there is the possibility of using "limb sounding".

Fig. 4.3

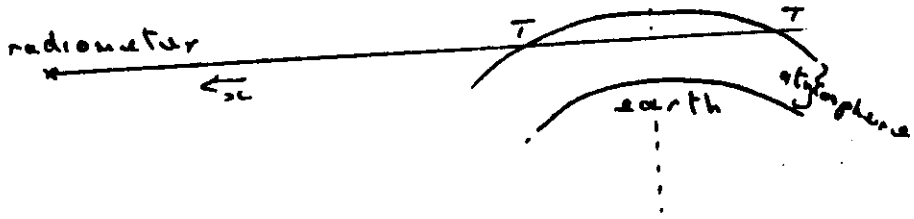

Here a radiometer with a very narrow angle of view observes the atmosphere tangentially. According to the earth + atmosphere radius employed so a weighting function is defined by the value of $\frac{\partial \tau}{\partial z}$ along TT and x may be expressed as a height co-ordinate above the surface of the earth. As the viewing angle is changed so a new weighting function is generated. These limb weighting functions are typically dominated by the contribution from close to the tangent point, as is shown in Fig. 4.4.

Fig. 4.4.

A set of weighting functions for a limb sounder with an infinitesimal field of view (after Gille and House, 1971).

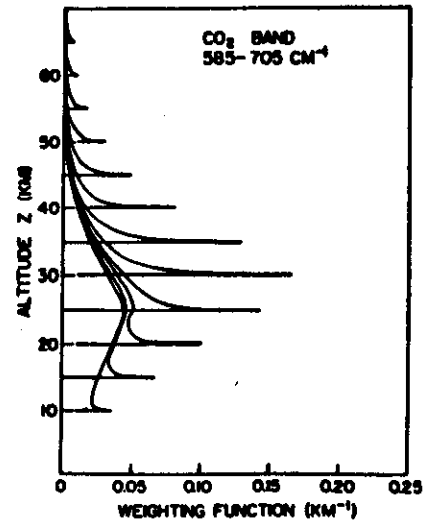

This allows a single band radiometer to define the stratospheric temperature profile. The temperature is determined first near the top of this atmosphere the viewing angle is then lowered towards the earth and the temperature of the next lower level calculated from the weighting function and the already determined temperature of the outer layer. This process is repeated for progressively lower layers. A major difficulty of this method is that the altitude of the satellite is not usually known precisely enough to define the height of the tangent point. One way of overcoming this is to use two radiometers with identical view angles

so $\frac{N_1}{N_2} = \frac{\int N_{B_1} K_1 d\nu}{\int N_{B_2} K_2 d\nu}$ where N_1, N_2 are the received radiances

If frequencies one and two are close

$$\frac{N_1}{N_2} \approx \frac{\int K_1 d\nu}{\int K_2 d\nu}$$

which is strongly pressure dependant so the height may be determined.

4.1.4. Instruments for atmospheric temperature sounding

Many types of special radiometers have been developed for temperature soundings all attempting to satisfy the desirable features of:

- a narrow spectral band which will give a peaked weighting function and good height resolution (required 200 mb)
- a narrow angle of view to give good spatial resolution
- a large energy capture to give good signal to noise ratio, so good temperature resolution (required 1K)

The main components of a radiometer are the receiving optical system, the filter and the detector. The geometry of the optical system and the size of the objective define the angle of view and the initial energy capture of the radiometer. Mirrors or germanium lenses are used for focussing the infra-red radiation.

Most of the scope for design variation comes in the filter design. Prisms and gratings may be used but give low energy availability, Fabrey-Perot interferometers give up to two orders of magnitude greater output while interference filters can give even more energy but have limited wavelength resolution. Each of these filters requires that either a separate optical system is used for each waveband or that observations are made sequentially. A Michelson interferometer may be used as a filter and the wavebands scanned by automatic variation of the difference in beam paths. An alternative filter system is to use

interference filters to select the broad band to be studied and to interpose a sample of the emitting gas in the received beam. This has the effect of cutting out most of the emission which originated high in the atmosphere by alternately interposing and removing such a cell. The alternating part of the signal corresponds to the emission from the upper atmosphere. The result is illustrated in figure 4.5.

Figure 4.5

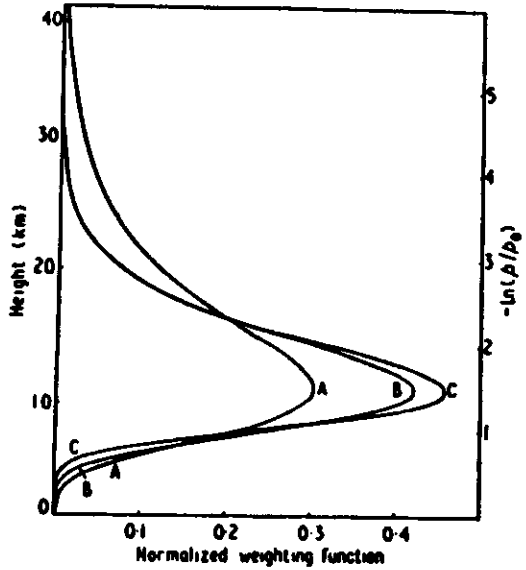

. . . Demonstrating the effect of selective absorption, weighting functions for: curve *A*, a 5 cm^{-1} wide interval near 690cm^{-1}; curve *B*, the same interval as for curve *A* but including a path of CO_2; curve *C*, an ideal weighting function for a monochromatic frequency in the wing of a spectral line (from Abel *et al.* 1970).

pairs of

By chopping between . . CO_2 cells containing different paths of CO_2 in the "selective chopper radiometer" a new of weighting function is generated.

Figure 4.7, transmission through two cells (or two pressures) near the centre of a single line in the CO_2 band (curves A and B). Curve C is the resultant transmission of chopping between the two.

Figure 4.8 shows the weighting function of a PMR operating in the CO_2 band with different cell pressures (in mb).

Figure 4.8

. Weighting functions for a pressure modulator radiometer having a cell 0.01 metre long operating in the ν_2 band of CO_2 with different cell pressures. The number of the curves is mean cell pressure in mbar (from Curtis *et al.* 1974).

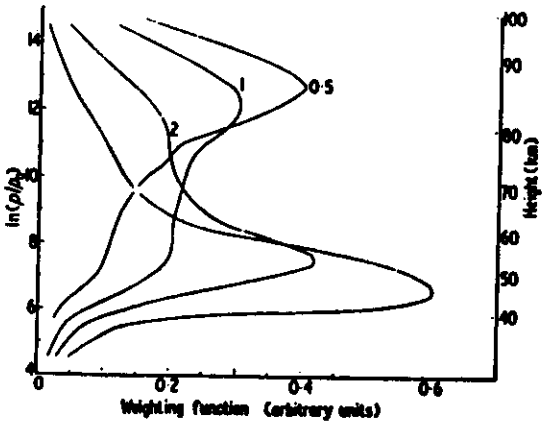

If the doppler principle is invoked a single cell of a PMR may give information on the vertical distribution of temperature. If the angle of view of the radiometer is changed from the vertical to looking ahead of the radiometer, the optical depth of the emitter is increased and the received frequency from it is doppler shifted relative to the PMR. This effectively creates a new weighting function. A set of such functions corresponding to different forward view angles is shown in figure 4.9 below.

Figure 4.9

. Weighting function for a pressure modulator radiometer housing a cell 1cm long containing CO_2 at a mean pressure of 0.5 mbar when viewing at different angles to the nadir, hence allowing scanning of the emitting lines from the atmosphere across the absorbing lines in the cell by the Doppler shift due to the relative motion between atmosphere and instrument. The number of each curve is the angle to the nadir in degrees (from Curtis *et al.* 1974).

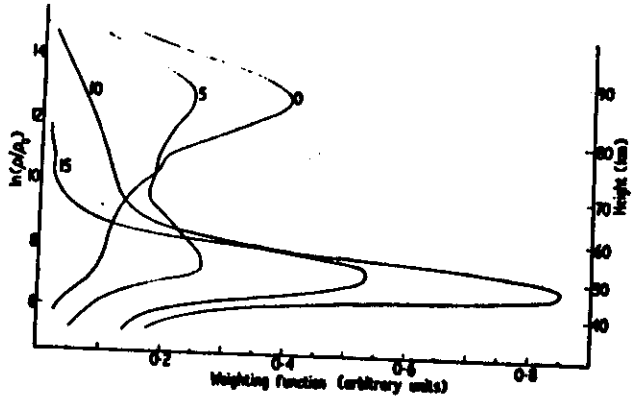

Microwave radiometers have also been used to measure atmospheric temperature profiles. Those operating in the 5mm O_2 emission band have the advantages of not being affected by cloud and of good spectral resolution allowing narrow frequency bands to be observed. However, the field of view is large ($\frac{1.2\lambda}{D}$ resolution) and the energy corresponding to atmospheric temperatures is small at these wavelengths.

4.2 Soundings for concentrations of atmospheric gases

Having discussed the sensing of atmospheric temperatures using techniques involving the emissions from gases with uniform distributions it is a parallel study to determine the vertical distribution of gases given the temperature distribution which may have been determined from remote sensing or other techniques.

For operational meteorological purposes the most important application is the measurement of water vapour profiles over the oceans. Here the wavelength used may be the 6.3 μm band to 20 to 40 μm band or many microwave bands.

As with temmperature soundings it is usual to take measurements of radiance at a series of narrow waveband intervals on the edge of an

absorption band. As the general shape of the humidity profile is usually known from climatological factors a first guess profile is taken and adjusted to fit the observed radiance/waveband pattern.

Figure 4.10

. Weighting functions for six channels of the SIRS on Nimbus 4 observing in the rotation water vapour band (from Smith 1970).

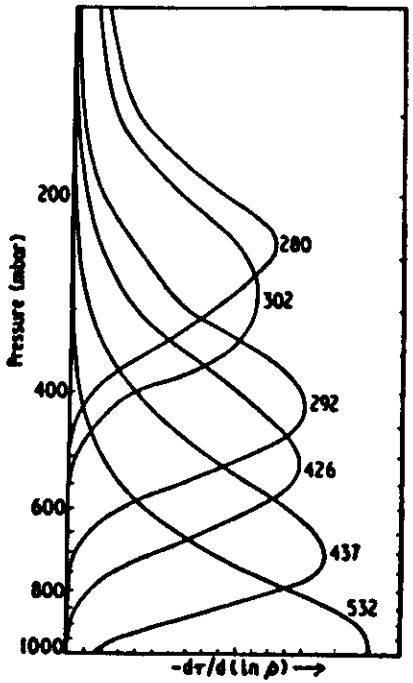

observing the apparent temperature of the earth's surface at two wavebands in the "water vapour windows". This technique is discussed in more detail in section 5 .

Microwave techniques are also used extensively for water vapour and liquid water determination. Early methods used single or double channel instruments in the 22 to 32 GHZ (about 1 cm) bands. At 22.235 GHZ there is a water vapour resonant absorption band with a minimum of absorption at 32.4 GHZ. Atmospheric transmissions in these bands range from 80% to 30% in the absorption band and 90% to 15% in the window. If the brightness temperature of the surface is known and is significantly different from the temperature of atmospheric liquid water or water

vapour the total atmospheric water can be deduced from the absorption of the surface radiation. The land typically has similar brightness temperatures to the atmosphere but the oceans having an emissivity of only about 0.45 are much colder ($\approx$ 130K).

Figure 4.11 below shows the calculted scene brightness temperatures for a range of microwave frequencies which would correspond to, no atmosphere, two specified total water vapour profiles in clear skies and one with a layer of stratus cloud present (Staelin et al 1976).

Fig 4.11

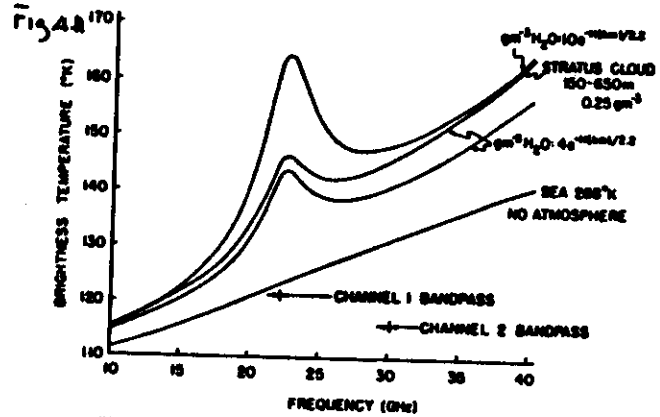

Theoretical microwave brightness temperature spectra computed for a nadir-viewing satellite over ocean at 286 K.

The water vapour content was estimated from linear combinations of the scene brightness temperature.

$V = -4.03 + 0.0841\ T_{B1} - 0.0515\ T_{B2}$

The result of experimental comparison of the microwave sounder with radiosound data is shown below.

Figure 4.12

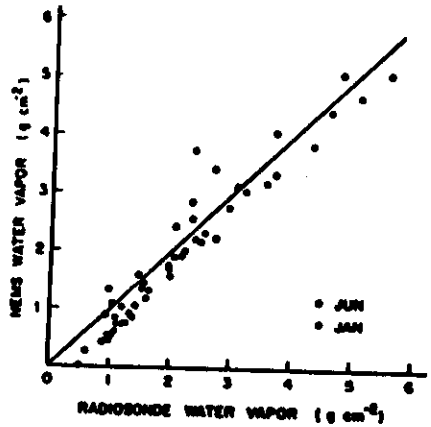

More recently research has been carried out into the use of the higher frequency water vapour absorption at 183 GHZ ($\approx$ 1.6 mm) which emit strongly enough for measurements to be made at several frequencies hence for a profile to be recovered. The weighting functions for a water vapour profile are shown in figure 4.13 alongside the weighting functions for a microwave temperature sounder operating in the 57 GHZ oxygen band.

Figure 4.13

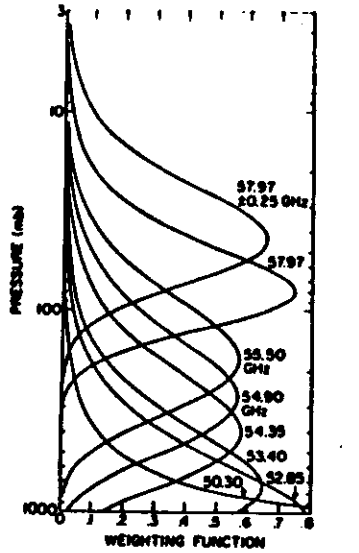

.. Temperature weighting functions in the oxygen band for vertical incidence.

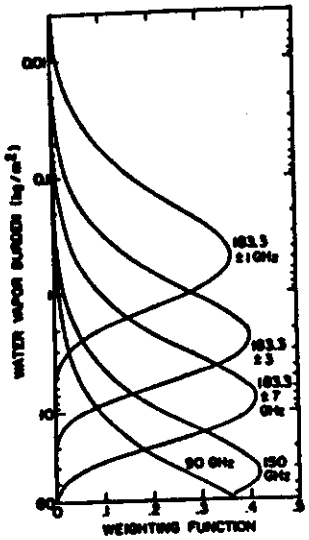

'. Temperature weighting functions near the 183 GHz water vapor line.

The water vapour burden assumes a climatological atmospheric pressure/water vapour relationship.

In the procedure developed by Rosenkranz et al the temperature/pressure profile was recovered from the O_2 band data and a temperature/humidity profile determined from the water vapour channel. The water vapour was then distributed according to pressure so as to reproduce the temperature/pressure profile.

Ozone concentrations are very important in stratospheric studies. Here limb sounding techniques can be used on the 9 to 10 μm ozone absorption band.

References:

Staelin, Kunzi, Pettyjohn, Poon and Wilcox, (1976), Remote sensing of atmospheric water and liquid water with the Nimbus 5 microwave spectrometer, J. App Meteor, 15.

Rogenkranz, Komichak and Staelin, (1982), A method for estimating atmospheric water vapour profiles by microwave radiometry, J. App Meteor, 21, 1364-71.

5. SOUNDINGS OF THE SURFACE OF THE EARTH.

5.1 THERMAL INFRA-RED SOUNDING OF THE SURFACE OF THE EARTH

The surface of the earth, and for the purposes of this discussion we include clouds as part of the surface, emits radiation in a continuum corresponding to a non-black body at around 300 K. The surface also scatters solar radiation selectively and measurements of the back scatter can provide information on the nature of the surface. There are also selective emission bands from water in the micro-wave region. Most of our efforts in sounding the earth's surface go to removing the effects of the intervening atmosphere and particulate matter.

Surface temperature measurements

Surface temperature data is used for estimating latent and sensible heat fluxes into the atmosphere over ocean and land surfaces, for cloud top height determination both for attribution of heights to wind vectors derived from cloud motion and for studies of convection.

Measurements of surface temperatures are usually made in the so-called "atmospheric windows", i.e. regions of the spectrum in which the atmosphere is relatively transparent. In the thermal infra-red bands these occur at around 11 μm and 4 μm, the latter, having overlap with the solar spectrum, cannot be used during daylight.

A radiometer operating over a defined waveband can only tell us what radiance is received over that band from the viewed surface. If the surface is black and there is no absorption or emission in the intervening atmosphere the signal from the radiometer can be interpreted as the surface temperature. The measured temperature is obtained either by calibrating the radiometer output against black body radiators at known temperatures or by inverting the Planck function corresponding to the observed radiance.

Figure 5.1

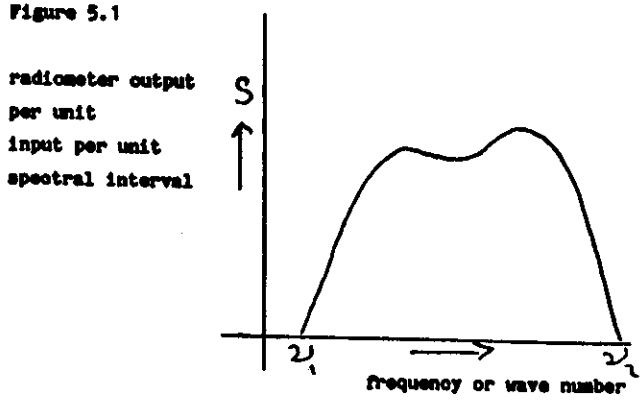

Radiometer output = $\int_{\nu_1}^{\nu_2} S_\nu N_\nu d\nu$

N_ν is the received radiance per unit spectral interval.

The normalized detected radiance N_N is given by

$$N_N = \frac{\int_{\nu_1}^{\nu_2} S_\nu N_\nu d\nu}{\int_{\nu_1}^{\nu_2} S_\nu d\nu}$$

Measured temperature = $\left[P^{-1} N_\nu\right]_{\nu_1}^{\nu_2}$

If the emitting surface is not black and there is no intervening absorption or emission then the radiometer will measure the "brightness temperature" of the surface and in general the brightness temperature will be a function of the radiometer acceptance band. If there is absorption between the radiometer and the surface the radiometer will indicate the scene brightness temperature. We try to recover the actual surface temperature from the scene brightness temperature by correcting for atmospheric effects and for the known radiative properties of the surface.

Figure 5.2

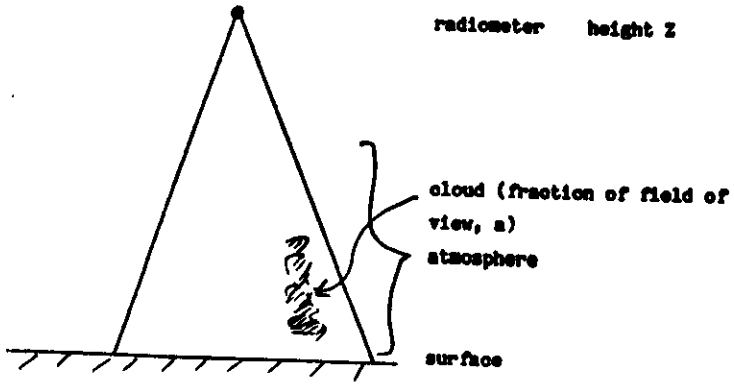

$$N = \epsilon_s N_{B_s} \tau_{(0,z)} (1-a) + \epsilon_c N_{B_c} \tau_{(c,z)} a + (1-a) \int_0^c N_{B_z} K_z dz + \int_c^z N_{B_z} K_z dz$$

N_λ = monochromatic radiation at the radiometer = $\epsilon_S N_{BS} (0,z)(1-a) + \epsilon_C N_{BC} (C,z) a + (1-a) N_{BZ} K_Z dZ + N_{BZ} K_Z dZ$

over the waveband of the radiometer the output will be

$$\int_{\lambda_1}^{\lambda_2} S_\lambda N_\lambda d\lambda \equiv \int_{\lambda_1}^{\lambda_2} S_\lambda N_{TB} d\lambda$$

where N_{TB} is the scene brightness temperature.

Our task is to extract the surface brightness temperature by removing atmospheric effects.

Assume (i) no cloud
(ii) a plane parallel atmosphere
(iii) the atmospheric absorption characteries are known.

The correction to be made for atmospheric abeorption and emission is not linear. The absorption depends on the properties of both the absorber and the surface radiance while the emission depends only on the amount and physical state of the absorber. In general analytical solutions to the atmospheric correction are difficult to find and finite element methods are used.

Dimer or e-type absorption

In the most frequently used atmospheric window (10 to 13 μm) the main absorber is water vapour and while the exact nature of the absorption has not been definitively described it is generally accepted to be due to clusters of water vapour molecules. It gives rise to a continuum of absorption and is subject to both foreign and self broadening. This is to say it is broadened both by the actual pressure of the atmosphere at which it exists and, separately, by the local water vapour pressure (hence e-type). It is also temperature and wavelength dependant.

Within the water vapour window the effective absorption coefficient is given by

$$k_\nu = k_{f,\nu}(T) \cdot p + k_{s,\nu}(T) \cdot e + k_{a,\nu}(T) p + k_{o,\nu}(T) f(p)$$

foreign broadening in continuum	self broadening in continuum	water vapour lines	other gases

dimer or e-type absorption which dominates.

Many empirical formulae describe the temperature dependance of the self broadening term which is ten or more times longer than the foreign broadening.

Figure 5.3 below shows experimental data on the wavelength dependance of e-type absorption.

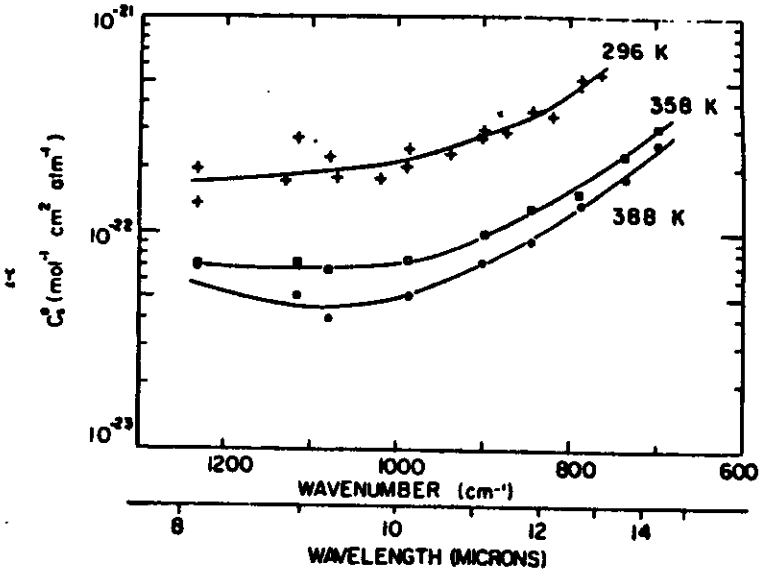

Comparison of the continuum absorption coefficient at three temperatures.

A scheme for determining the atmospheric correction is as follows.

1) Divide the waveband of the radiometer into intervals such that both the sensitivity of the radiometer and the Planck function at surface and atmospheric temperatures vary only slightly across the interval.

2) a) Divide the atmosphere into plane parallel layers $\Delta\tau$ of a thickness such that the absorber amount in each layer is small enough for $e^{-k\rho\Delta z} \approx 1 - k\rho\Delta z$

b) starting at the top of the atmosphere calculate for each wavelength interval

(i) the transmission and absorption of each layer

(ii) the transmission and absorption to the top of the atmosphere from each layer

(iii) the emission from each layer

(iv) the outgoing radiation from each layer

(v) the outgoing radiation from the surface for a series of assumed surface temperature

(vi) the total outgoing radiation.

3) Sum the products of the total outgoing radiation and the radiometer sensitivity for all intervals to calculate the radiometer output.

We then produce a "look-up" table of scene brightness temperatures (measured temperatures, T_M) and the corresponding surface brightness temperatures (T_S) for that atmospheric water vapour and temperature profile. This table is used to interpolate T_S from the T_M which was actually measured. The difference ($T_S - T_M$) is often referred to as the temperature deficit (ΔT) or the atmospheric correction. Under tropical conditions with dry soils the deficit may exceed 30 deg K.

Split window techniques for estimating atmospheric corrections

In the absence of atmospheric temperature and humidity data it is possible to estimate the correction to within about 10% if data from two infra-red channels are available. Because the absorption by the atmosphere is wavelength dependant two radiometers viewing the same scene at different wavelengths will record different scene brightness, (or measured) temperatures (T_M). Within a climatic zone, season or synoptic situation the difference between the two measured temperatures taken with either one of them gives a unique (but approximate) relationship to the surface B.T. This is illustrated below for conditions typical in the wet season in the Sahel zone of West Africa.

Figure 5.4

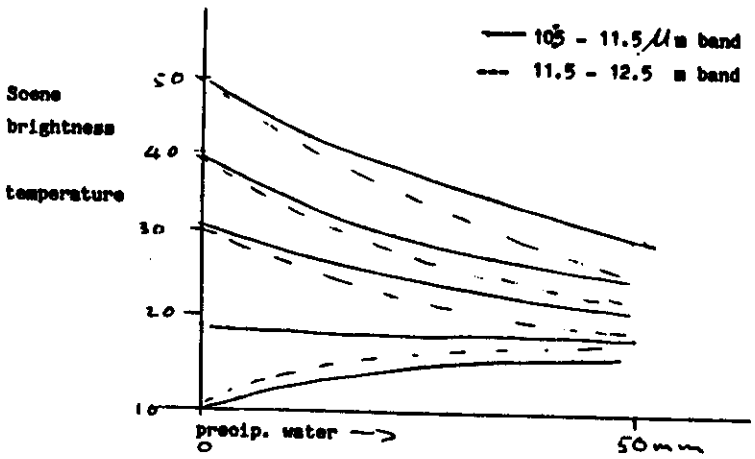

It is assumed that the surface emissivity is constant across the two wavebands.

5.2 VISIBLE WAVEBAND SOUNDINGS OF THE EARTH'S SURFACE

5.2.1 Reflected or back scattered solar radiation may be measured by satellite borne radiometers. Spectral measurements are used to identify surface characteristics while data for the whole band is needed for energy studies.

Figure 5.5

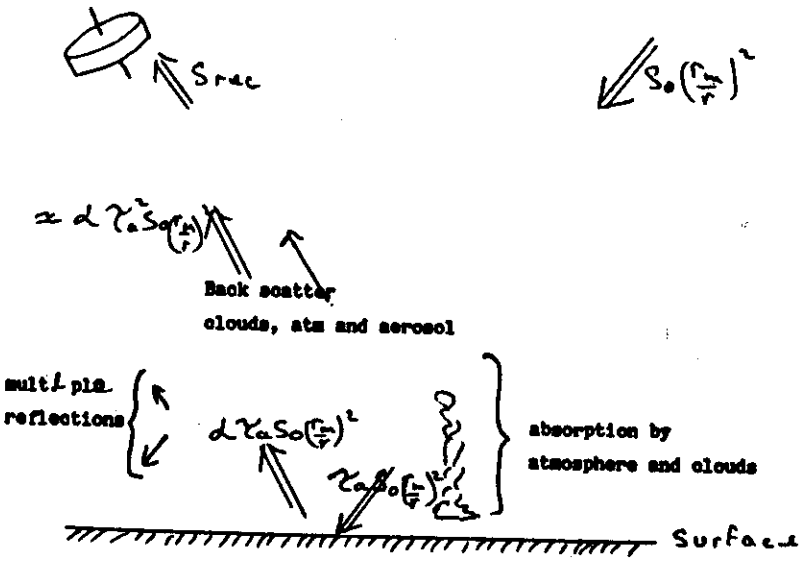

τ_a includes atmospheric absorption and scattering effects

α the surface reflection coefficient

= α(surface type, angle of incidence
angle of view of radiometer, frequency)

$\frac{S_{rec}}{S_0\left(\frac{r_m}{r}\right)^2} \equiv$ global albedo

5.2.2 Surface cover determination

Different surface types reflect differently in the different parts of the spectrum. Because of atmospheric effects it is often difficult to measure the reflectance of the actual surface. It may be easier to measure the ratio of the reflectance in two parts of the spectrum assuming that the relative atmospheric effects are similar in both parts. One of the main applications of these techniques is in detecting the

presence of green vegetation which absorbs strongly in the red and only about 50% in the near infra-red. The presence of green vegetation is now of interest to meteorologists as it implies transpiration of water into the atmosphere. Figure 5.6 below shows the spectral reflectance curves of various typical ground cover types and the channels available on the LANDSAT and NOAA AVHRR radiometer bands.

Fig 5.6

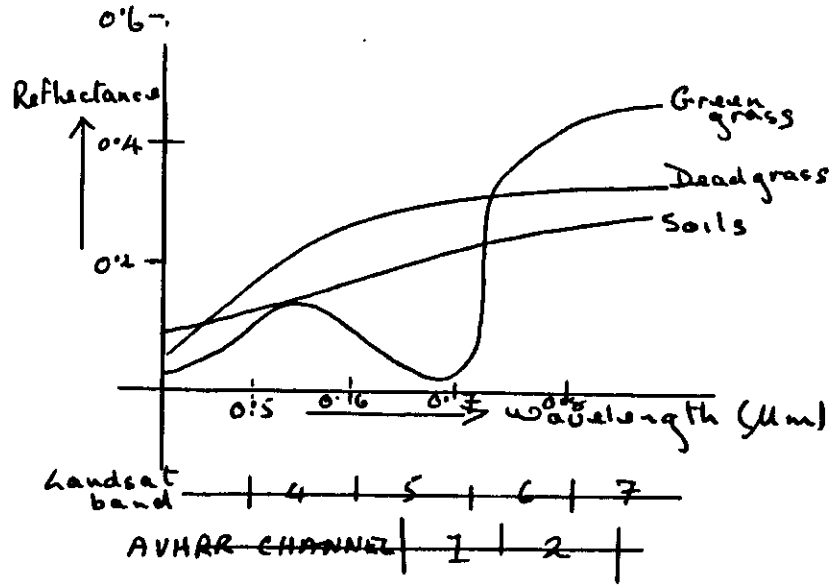

Many different types of ratioing techniques have been devised and tried. The most widely used for vegetation mapping is:

$$\frac{\text{near infra-red} - \text{red}}{\text{near infra-red} + \text{red}}$$

It is seen that using the AVHRR this gives values close to zero for soil, 0.25 for dry grass and 0.6 for green grass.

5.2.3 Qualitative uses of visible data

Satellite imagery in the form of photographic or similar copy has been used for many years to identify and monitor synoptic and sub-synoptic scale meteorological features. Visible band imagery offers generally higher resolution than the infra-red imagery because the energy available allows higher resolution radiometers to be used. This course will not deal with satellite image interpretation but it should be noted that the combined use of thermal infra-red and visible data enhances the value of the data many-fold. Also, as image processors become cheaper and more readily available it is becoming possible to view the data with much better resolution than has been possible previously. This gives greater insight into the structure and development of meteorological features.

5.3 Microwave soundings of the earth's surface.

5.3.1 General

Microwave soundings may, like VIS and I-R, be passive but we have here the opportunity of also using active systems and observing the reflectivity of features in the micro-wave frequencies.

One limitation of passive microwave sensing is that of spatial resolution. Often the resolution available, even from satellites in orbits as low as 300 km is less than the scale of the feature we wish to observe.

Figure 5.7 shows the opacity of the atmosphere in the microwave region and Fig. 5.8 indicates the frequency ranges of some remote sensing applications.

Figure 5.7

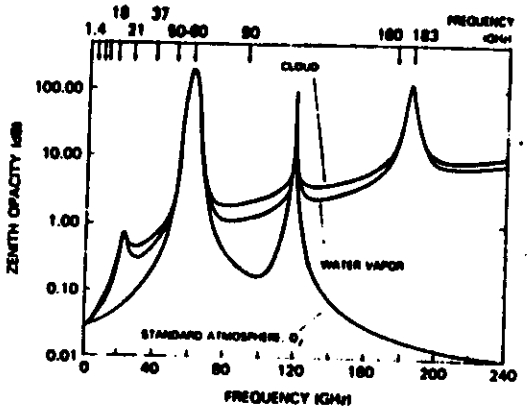

Microwave absorption in the atmosphere. Lower curve - atmospheric opacity due to oxygen. Middle curve - opacity with 20 kg m^{-2} water vapour added to the oxygen. Upper curve - opacity with 0.2 kg m^{-2} stratus cloud added to the oxygen and water vapour.

(From HMMR vol IIe, NASA 1987)

Figure 5.8

Physical Observable	Frequency of Observation (GHz)									
	1.4	6	10	18	21	37	50-60	90	160	183
Soil moisture	●	O								
Snow		O	O	●		●		●		
Precipitation Ocean			●	●	O	●				
Land				●		●		●		●
Sea surface temperature		●	●	●	●	O				
Sea ice Extent				●		●		O		
Type		O	●	●		●		●		
Wind speed (sea surface)			●	●	O	O				
Water vapor Total (over ocean)				●	●	●				
Profile					●	O	●	O	●	●
Cloud water (over ocean)					●	●		●		
Temperature profile					O	O	●	O		

Key: ● Necessary ● Important O Helpful

Parameters which are measured with microwave sensors and the frequencies at which the measurements are made.

(from HMMR vol IIe, NASA 1987)

5.3.2 Passive microwave soundings of soil moisture.

The moisture of the soil influences the strength of the microwave emissions from it. However, the temperature of the soil, the vegetative cover and the roughness of the surface influence the energy reaching the atmosphere through the emission, absorption and emissivity respectively. The vegetative effect increases with frequency so long wavelengths are preferred (~ 1.4 GHz). Moisture in the upper 5 cm of the soil contributes to the emmission at this wavelength. For this data to be of any practical use it has to be used in models of soil moisture using known or assumed physical properties of the soil. Research in this field continues but has not yet reached an operation state.

5.3.3 Microwave detection of snow and ice.

The 18 & 37 GHz frequencies can be used to detect the presence of dry snow because of its unusually low emissivity at these frequencies. Cloud has little influence on the measurements. If the snow is melting confusion with bare ground may result. Similarly ice fields can be identified over the oceans. Here the contrast between emissivity of dry ice and liquid water makes delineation easy.

5.3.4 Microwave soundings of sea state and winds over the ocean

The emissivity of the sea surface varies with its roughness (small scale) hence with the wind speed.

Both speed and direction can be deduced if a sideways looking active microwave system is used. Such a technique was employed in the SEASAT-A-Scatterometer System (SASS). A 14.6 GHz signal is reflected mainly by the capillary (order 1 cm) waves on the sea surface. The roughness on this scale depends on the wind close to the surface. By using the doppler shift of the return signal caused by the satellite's motion the resolution of the data could be increased to about 50 km. Empirical relationships were established between surface wind speed and direction and back scattering as a function of elevation and azimuth relative to the satellite and the polarisation of the backscattering.

6 - FURTHER APPLICATIONS OF SATELLITE DATA IN METEOROLOGY

6.1 Wind finding

6.1.1. Tropospheric winds

Over the oceans the tracking of clouds in either or both the visible and thermal infra-red channels offers a ready means of assessing wind speeds. It is assumed that the clouds are moved by the wind at about the level of their tops. This level is determined from the cloud top temperature and climatic or synoptic data about the atmospheric temperature profile. Many schemes involving automated or manual pattern recognition techniques have been developed for calculating satellite cloud tracking, most involve interactive image processing. A fairly typical method is outlined below.

Figure 6.

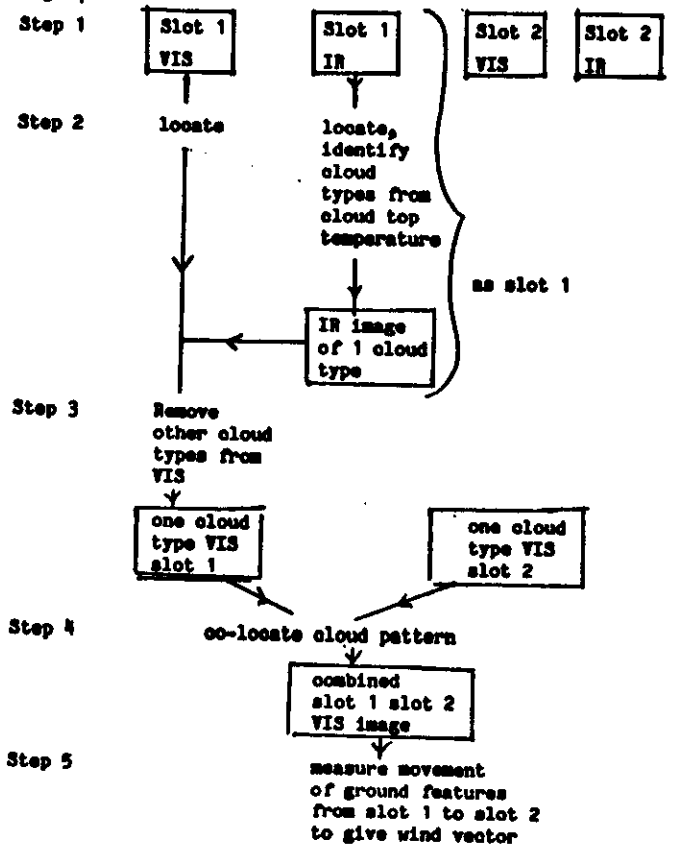

Steps 3 to 5 are repeated for each cloud level present.

Areas of about 1° square are treated at a time. Low level winds from stratocumulus or cumulus cloud movement have standard errors of about 1.5m s^{-1} while high level winds from cirrus tracking give errors of about 2.0 m s^{-1}.

6.1.2. Surface wind

Satellite borne radar has been used in an experimental mode to measure surface winds over the ocean. The SEASAT-A scatterometer system (SASS) detects the small scale roughness of the ocean surface from the increased radar back scattering, the change in polarisation and the doppler shift of the back scattered signal indicate the direction of the wind relative to the satellite. The surface roughness is correlated with the wind speed empirically. Results indicate that winds may be measured to + 2.0 m s^{-1} in strength and to + 20° in direction.

6.2 Rainfall estimation from satellite data

6.2.1. Microwave techniques

The most promising technique for rainfall estimation is the, as yet experimental, one using microwave emission to detect the presence of liquid water in clouds.

6.2.2. Infra-red and visible techniques

As there is at present no commitment for operational meteorological satellites with microwave channels suitable for rainfall estimation, methods using the currently available visible and thermal infra-red channels have been developed experimentally and have had limited operational use.

These methods rely on recognising the thermal I-R and VIS imagery the main characteristics of rain producing cloud systems. Large liquid water content gives rise to high reflectance in the visible channel and clouds reaching high levels in the atmosphere such as cumulonimbus can be recognised in the thermal I.R.

Figures 6.2. a, b, and c below illustrate these characterics.

Fig.6.2. Joint frequency distribution of SMS-1 visible and infrared data for a 400 x 400 km box centred at 09°00'N, 22°40'W in the eastern tropical Atlantic Ocean, 1300 GMT 5 September 1974. Data have been normalized to a scale 0-1. (a) No rain case (N class). (b) Rain case (R class). After Lovejoy and Austin, 1979a. (c) Conditional probability of rain based on (a) and (b).

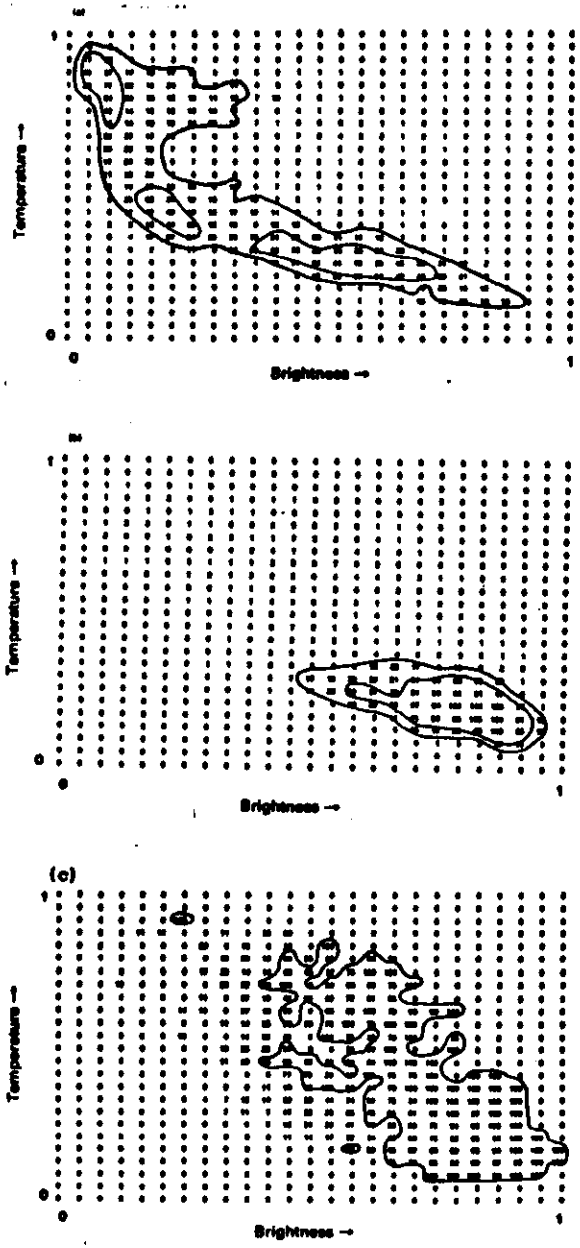

The interpretation of the clouds VIS and/or I.R. features in terms of rainfall has followed two principle lines. First, the use of high quality photographic type imagery to recognise typical rain bearing systems and to attribute rainfall amounts to them according to their persistance over an area and the climatologically expected rainfall from such systems. These methods have achieved some success particularly when used as interpolation schemes between raingauges and when applied to large scale synoptic rainfall events which give rise to relatively homogeneous rainfall at the ground. The second method, more suitable for convective rainfall, consists of monitoring the development of clouds using digital I-R data sometimes in conjunction with the visible data. It is found that convective systems give most of their rainfall in their growth stage and that having reached their maximum horizontal extent generally give little precipitation. Figure 6.3. below illustrates this.

Fig. 6.3. The area of rain producing cloud (A_r) a function of the size of the cloud (A). Both scales are normalized by the maximum size the cloud attains (A_m). The curves represent clouds of three different size ranges. (after Barrett and Martin, 1981).

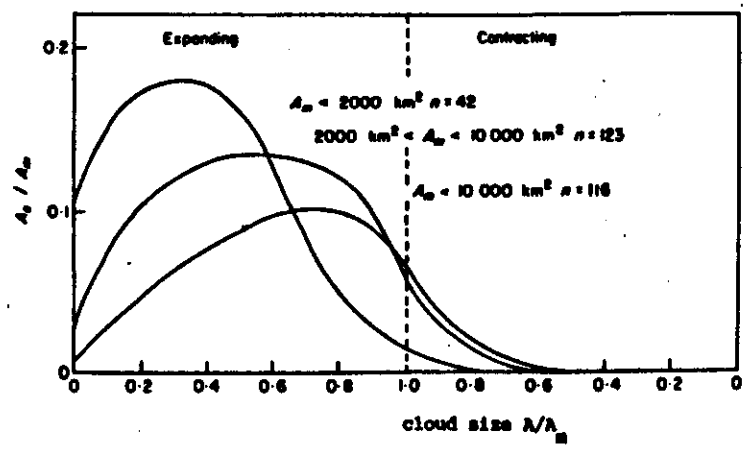

The implication of the above is that convective systems must be monitored each hour or so if reasonable estimates of rainfall from them are to be made. Hence, data from geostationary satellites must be used. Only the I-R channel can monitor their activity during the night. Most experimental and quasi-operational models employ a rainrate (R) equation of the form:

$$R = a_0 + a\frac{\partial A}{\partial t}\cdot\frac{1}{A} + \text{additional terms}$$

where a_0 implies the presence of cold cloud below a predetermined temperature (temperatures from 223 K to 243 K have been used) and $\frac{\partial A}{\partial t}\cdot\frac{1}{A}$ is the rate of growth of the area of cloud below that or another predetermined temperature. The additional terms may include such factors as storm propogation or decay. All these schemes are empirical and the coefficients established for one climatic region are not universally applicable; for instance those developed for convective storms over the tropical Atlantic Ocean proved inappropriate over continental West Africa.

Estimates of rainfall from tropical convective systems over long periods (30 days) or over large areas may be achieved without the inclusion of the growth term in the above equation. One is then left with the rainfall being related to the persistance of clouds of convective origin over a site or the mean fractional cover over an area. The implication is that, in the absence of orographic effects, when averaged over a number of rainfall events a site would experience some storms in each phase of growth or decay. Figure 6.4. shows a contingency table for the rainfall and persistance of cold cloud over sites in the Republic of Niger in

Figure 6.4.

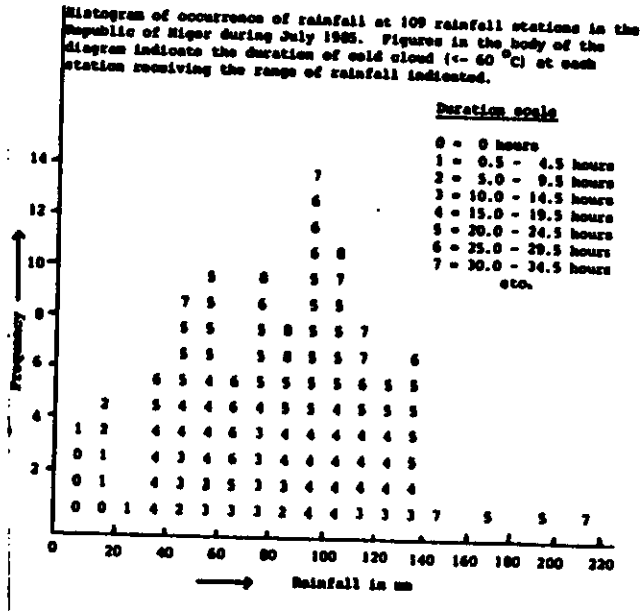

In interpretting such diagrams it is necessary to recall the large spatial variability of rainfall from these storm systems. Typically rainfall from large systems will vary by a factor of two over distances of ten kilometers. Hence raingauge data can only be used in a statistical sense to calibrate satellite estimates and similarly a satellite estimate that gave an accurate mean rainfall over a 5 km x 5 km pixel would have to be interpretted in terms of a widely spread rainfall distribution within that pixel.

6.3 Soil moisture and evaporation measurement from I-R and VIS satellite data

Techniques for the estimation of soil moisture and evaporation from satellite data are generally based on surface energy budget (SEB) concepts and involve the use of both satellite and surface data.

The SEB may be written

$$R_N = H + \lambda E + G$$

- R_N: net radiation towards the surface
- H: sensible heat flux from the surface
- λE: evaporative heat flux from the surface
- G: ground heat flux from the surface

with $R_N = S(1-\alpha) + L\downarrow - L\uparrow$

- $S(1-\alpha)$: absorbed solar radiation
- $L\downarrow$: downwards long wave radiation
- $L\uparrow$: upwards long wave radiation

The solar radiative term may be estimated from the visible channel data using climatological data for the atmospheric absorption loss. The long wave radiative terms can be calculated from satellite measured atmospheric and surface temperatures. If clouds are present cloud base temperatures must be estimated.

The heat flux terms are usually expressed in resistance terminology

$$H = \rho c_p \frac{T_s - T_a}{r_a} \quad ; \quad \lambda E = \rho \frac{c_p}{\gamma} \frac{(e_s - e_a)}{r_a}$$

$$G = k \frac{\partial T}{\partial z}\Big|_{z=0} \text{ with } C\frac{\partial T}{\partial t} = \frac{\partial}{\partial z}\left(k \frac{\partial T}{\partial z}\right) \text{ in the soil}$$

where r_a is an aerodynamic resistance which depends on wind speed and vertical temperature gradient, k is the thermal conductivity of the soil and C its volumetric thermal capacity. C is slightly dependant on soil moisture content and k strongly dependant.

If surface synoptic data (T_a, e_a, u_a) are available H may be calculated. The vapour pressure at the gound surface (e_s) is not usually known but it may be related empirically to the saturated vapour pressure at the earth surface and the difference in temperature between the surface and the air. Another approach to the λE term is to express it as

$$\lambda E = \rho \frac{c_p}{\gamma} \frac{(e_\delta - e_a)}{r_a + r_\delta}$$

where δ is the depth below the soil surface at which water is available for evaporation, e_δ is then the saturated water vapour pressure at the temperature corresponding to that depth. Models to solve these equations

using up to twentyfour data points per day have been developed. Other models assume all changes to be cyclic and use only two data points per day. Over bare soils with high insolation evaporation is controlled almost entirely by the resistance to vapour diffusion through the dry upper layer of soil. Under these conditions for a specified type of soil the diurnal range of surface temperature reflects well the depth of the dry layer and hence the availability of water for evaporation.

Figure 6.5 illustrates the effect on the diurnal range of temperature of a bare soil surface of irrigation and shows the rate of recovery of the temperature cycle towards the dry condition as water evaporates through the upper layers. This is the basis of one method for the estimation of soil moisture in the upper layers and of evaporation from satellite data.

Fig. 6.5

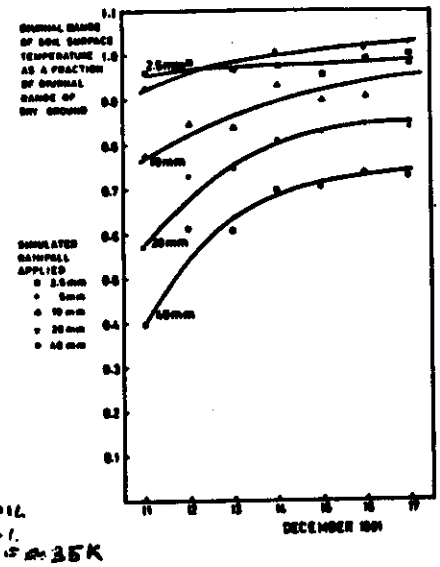

There are at present at least six models being tested for evaporation and soil moisture monitoring but none appear to have yet reached an operationally viable state.

7. ELEMENTARY RADAR METEOROLOGY

Radio Detection And Ranging

Radar consists of the use of a microwave (0.1 to 100 cm wavelength) signal generator and receiver to detect the presence, bearing, and range of a back scattering target and perhaps to make deductions about the nature and movement of the target.

Radar is used in meteorology for:

Wind finding - by tacking balloon borne targets.

Storm detection and tracking by back scattering from raindrops.

Rainfall estimation - from the strength of the return signal.

Cloud physics research.

Turbulence detection.

Sea state - hence surface wind.

7.1 The principles of radar

The main components of a simple radar are illustrated below.

Fig. 7.1

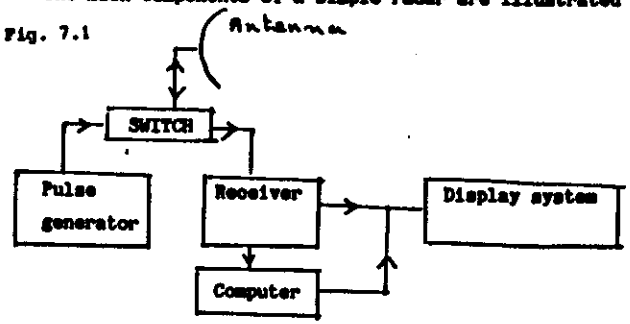

The pulse generator produces fixed (or dual) frequency high energy pulses of microwaves. Pulses typically last μs and are repeated in ms. The wavelength may vary from a few mm to a metre but the most frequently used are in the range one to twenty cm. Pulse length is about 100 m.

The switch automatically disengages the receiver from the antenna while a pulse is being transmitted.

The antenna is a parabolic dish or section thereof with the transmitting and receiving terminals at its focus so that a quasi parallel beam is produced. The focussing power depends on the wavelength and the diameter of the dish. Antenna may have the capability of being locked onto a target so that they can track objects. This is usually used in windfinding applications.

For storm tracking or storm monitoring purposes antenna may rotate continuously so scanning the area within range ($\sim$200 km) or they may scan in a vertical direction so as to give a vertical section of a particular storm. The latter is known as the "nodding mode."

The receiver is a tuned amplifier. The sensitivity of the radar is determined by the minimum detectable signal. Because of the varying range of the targets and their different back scattering properties the strength of the received signal varies by many orders of magnitude so some selective amplification system is needed. Receivers may be able to detect the doppler shift of the signal by comparing its frequency to that of the transmitted pulse.

The indicator is the means of displaying the target. Early radars had either plan position indicators (PPI) for use with the antenna in the rotating mode or range height indicators (RHI) for use with the antenna in the nodding mode. The P.P.I. in its simplest form was a cathode ray tube with a time base which was triggered from the centre of the screen each time a pulse was transmitted and which rotated at the same speed as the antenna. Hence the received signal appeared as a spot at a distance from the centre of the screen proportional to the distance of the target from the radar and orientated in the same direction as the target. The R.H.I. has also the centre triggered time base but in this case the time base nods in unison with the antenna so that a precipitating cloud is seen as a vertical bright band at a distance from the screen centre proportional to the distance of the cloud from the radar.

Many modern radar sets computer process the return signal so that it can be displayed on a colour V.D.U. with colours indicating the strength of the scattering source and the position indicated on any convenient map projection.

7.2 Some radar characteristics

The minimum range is determined by the pulse length (the set cannot receive while a pulse is being transmitted) and is equal (& just over) half the length of the pulse (typically 200 m)).

The maximum range is limited by the power of the radar, the curvations of the earth, the strength of the back scatterer and by the pulse repetition frequency (PRF). The latter because if a signal is received at a time greater than $(PRF)^{-1}$ after transmission the range will be incorrectly indicated.

The position of the target is uncertain within the "rise time" of the pulse. This is the time for the pulse to achieve its maximum amplitude. One tenth of a μs rise time introduces an uncertainty of 15 to 30 m in position.

The beam width determines the directional accuracy of the radar.

Fig. 7.2

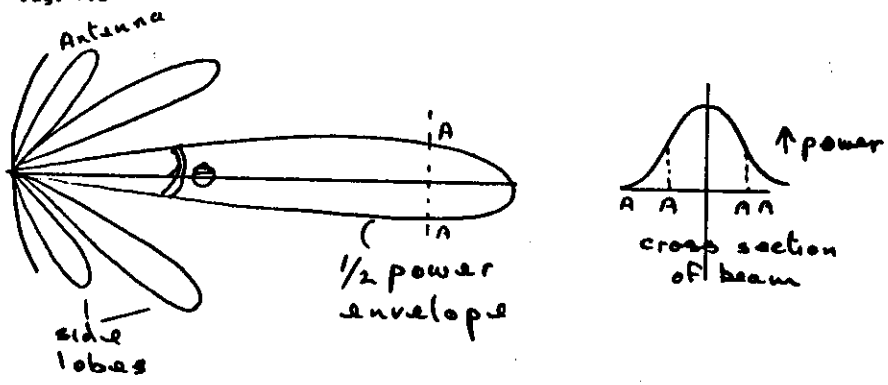

Typically for a ground based radar a beam width is about 1^0. If high directional accuracy is needed either a rotating or nodding source is used at the focus. This gives a return signal which peaks each time the centre of the beam passes the target and the maximum position is noted. Such systems give directional accuracy to 10^{-2^0}.

Refraction of the radar beam by atmospheric temperature and humidity gradients. Under "normal" atmospheric conditions the radar beam is curved towards the earth. To simplify calculations of the height of the beam above the ground it is easiest to assume a straight beam and adjust the apparent radius of the earth. In these "normal" conditions a factor of about 4/3 can be used. If temperature inversions and strong humidity gradients are present the radius of curvature of the beam can be reduced to that of the earth giving rise to the phenomenon known as ducting.

Refraction of E - M radiation

Fig. 7.3

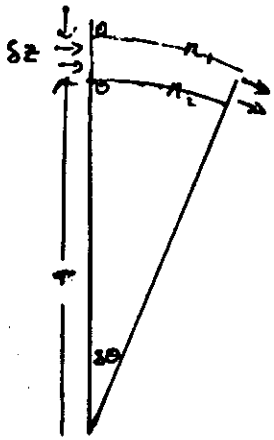

Consider a plan wave front OO propogating in a stratified medium. If n decreases with height the wave front will tend to tilt as it propogates.

$$\delta\theta = \frac{c\delta t}{n_1}\cdot\frac{1}{r} = \frac{c\delta t}{n_2}\frac{1}{(r+\delta z)}$$

$$r n_1 = (r+\delta z)(n_1 + \delta z\frac{\partial n}{\partial z})$$

$$0 = n_1\delta z + r\delta z\frac{\partial n}{\partial z} + \delta z^2\frac{\partial n}{\partial z}$$

$$r = -n/\frac{\partial n}{\partial z}$$

In air n = 1.0003, so $r = \left(-\frac{\partial n}{\partial z}\right)^{-1}$

$$n = a\rho_a + b\frac{\rho_w}{T}$$

	Visible	Microwave
a	$\sim 2.28\times10^{-4}$	2.23×10^{-4}
b	0	1.77

EX

Show $$\frac{\partial n}{\partial z} = \frac{-p}{RT}\left[\frac{\partial T}{\partial z}\left(a + \frac{bq}{T}\right) - b\frac{\partial q}{\partial z} + \frac{q}{T}\left(a + \frac{bq}{T}\right)\right]$$

Hence find the temperature and humidity lapse rates near the earth's surface which would keep a radar beam // to the surface.

7.3 The radar equation

Fig. 7.4

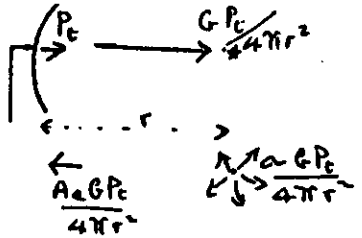

Pt, peak power transmitted

G, aerial gain $\approx A_e \frac{4\pi}{\lambda^2}$

Ae, effective area of aerial
2/3 actual area

σ back-scattering cross section of target.

$$P_r = \frac{P_t \sigma G^2 \lambda^2}{(4\pi)^3 r^4} = \frac{P_t}{4\pi} \frac{\sigma}{r^4} \frac{A^2}{\lambda^2} \cdot \frac{4}{9}$$

Typically for ground based radar
$P_t = 10^6 w$, $A \sim 4 m^2$, $\lambda = 0.1$ to $0.01 m$, $P_{r(min)} \sim 10^{-15} w$

The factor $G = A_e \frac{4\pi}{\lambda^2}$ is true on the beam axis but the cross beam power curve is Gaussian so for extended targets a correction factor $\pi^2/32 \ln 2$ should be applied.

Targets may be:

metal reflectors - for wind finding;

hydrometeors - for storm warning and rainfall measurement;

waves - for sea state and surface wind.

7.4 Scattering

Scattering is the interaction between particles and E-M radiation which results in changes in direction (and polarisation) but not in the energy or wavelength of the incident radiation.

The back scattering cross section σ of a target is the cross sectional area of the isotropic scatterer would have which returned to the antenna the same energy as the actual scatterer: may be many times or a small fraction of the actual cross section of the target.

Mie and Rayleigh scattering if the scatterer is small compared to the wavelength then the Rayleigh scattering regime will prevail. This is usually the case in the detection of hydrometeors by radar.

See over page

Fig. 7.5

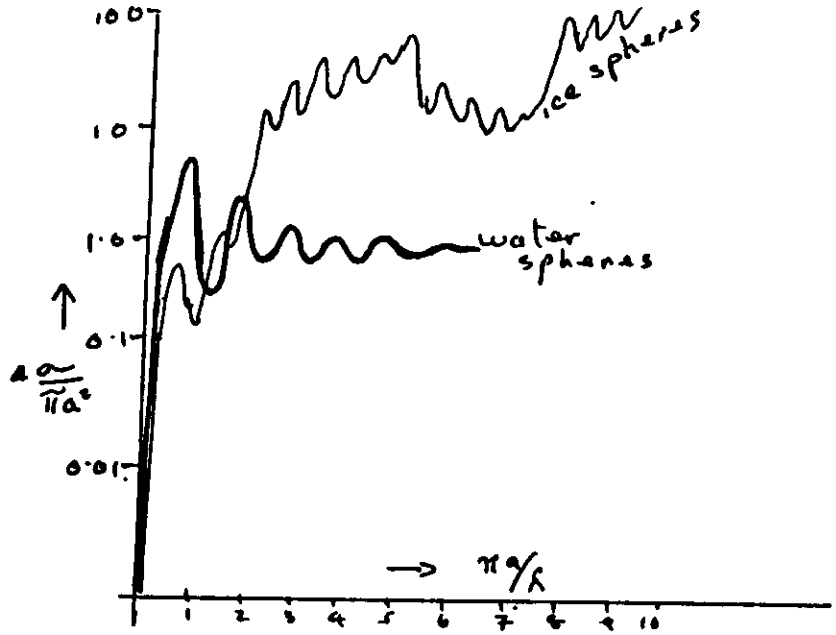

Scattering by spherical particles

The figure shows the full range of scattering regimes from spherical particles; a is the diameter of the actual scattering. Note that water is a relatively better scatterer than ice for all except large hail. Also, for most particles $\pi a/\lambda < 0.5$ the increase in the ratio of back scattering to actual area is smooth. This is the Rayleigh regime.

If $a \ll \lambda$

$$\sigma \approx \left(\frac{\lambda}{\pi}\right)^2 \left(\frac{\pi a}{\lambda}\right)^6 \left(\frac{n'^2-1}{n'^2+2}\right)^2 \quad \text{where } n' \text{ is the complex refractive index}$$

$$\approx \frac{\pi^5}{\lambda^4} \frac{(n'^2-1)^2}{(n'^2+2)^2} 2a^6$$

Put $\left(\frac{n'^2-1}{n'^2+2}\right)^2 = |K|^2 \begin{matrix} = 0.93 \text{ for water} \\ = 0.20 \text{ for ice} \end{matrix}$

In terms of drop mass (m)

$$\sigma = \frac{\pi^3}{\lambda^4} |K|^2 \frac{m^2}{\rho^2} \cdot 36$$

The power received from a volume containing spherical particles which fills the radar beam

$$\overline{P_r} = \frac{P_t G^2 \lambda^2 \pi^2}{(4\pi)^3 r^4 32 \ln 2} \cdot \underbrace{\frac{h}{2} \frac{4\pi r^2}{G}}_{\text{volume irradiated}} \frac{\pi^5}{\lambda^4} |K|^2 \sum_{\text{unit vol.}} (a^6)$$

$$= \frac{P_t C h \pi^5 |K|^2}{r^2 \lambda^2 2^8} \sum_{\text{unit vol}} (a^6)$$

$$= \frac{C K^2 \sum (a^6)}{r^2}$$ where C is a constant of the radar

Back scattering by melting ice spheres

Fig. 7.6

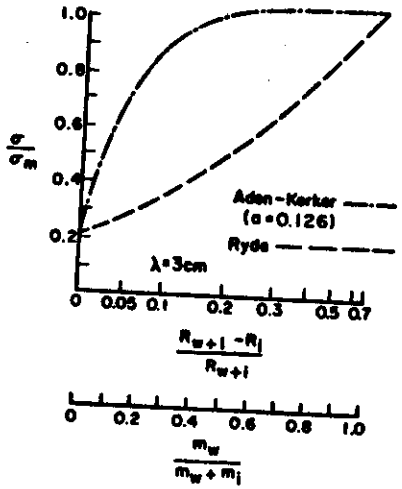

Variation in backscattering of a melting ice sphere as a function of melted mass. *dashed curve*, results of calculations from Ryde's theory, which assumes that the particle consists of a homogeneous mixture of water and ice; *dot-dash curve*, a shell of water surrounding an ice sphere. From Langleben and Gunn (1952).

$\frac{m_w}{m_w + m_i}$ = relative water mass to total hydrometeor mass

We see a fourfold increase in back scattering when 10% of an ice sphere melts. This accounts for the "bright-band" often observed on R.H.I. by radar when viewing around the freezing level.

Back scattering by small non-spherical particles

Except for light rain and drizzle water drops are non-spherical, neither in general are ice crystals. Falling raindrops are usually oblate with the minor axis vertical, on reaching their maximum size before break-up they resemble an inverted saucer with a thick rim.

The effect on back scattering of their distortion is to increase the dipole moment of the particle hence its back scattering cross section.

Figure 7.7 below shows the increase in σ of an elipsoid for a non-polarized 10 cm radar.

Fig. 7.7

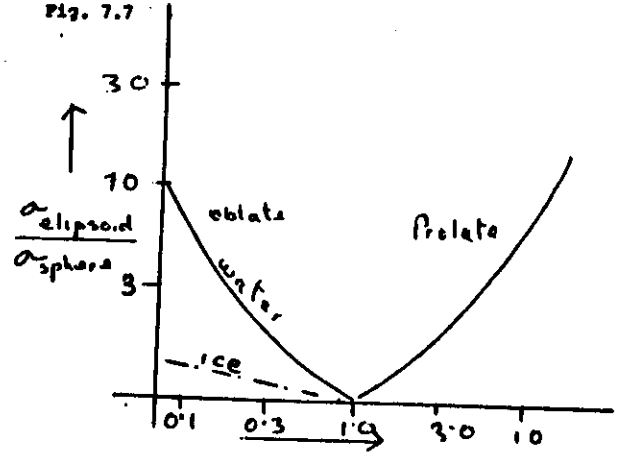

(From Battan) after Atlas

3 - RAINFALL MEASUREMENT BY RADAR

$P_r = \frac{c}{r^2} K^2 \sum_{\text{unit vol.}} a^6$ for an assembly of spherical scatterers.

To apply this equation to rain rate measurements we must take account of:

non spherical scatter;

is K ice or water?

possibility of non Rayleigh scatter;

attenuation of the radar beam;

rain rate/drop size distribution relationships;

the effect of vertical air motion.

To achieve this we substitute Z for a^6 and search for the relationship between Z, which is known as the radar reflectivity factor, and the rainfall rate (R).

3.1 Drop size distribution

The processes determining the distribution of drop sizes are mainly the growth by coalescence and the spontaneous break-up of large drops. One of the classical drop size distribution measurements, made by Marshal and Palmer (1948), is illustrated in fig. 4.1

Fig. 8.1

(From Doviak)

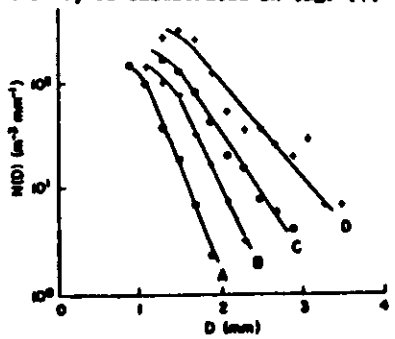

Raindrop size distribution versus drop diameter. (Data from Marshall and Palmer, 1948.) Curves ABCD are for rainfall rates of 1.0, 2.8, 6.3, and 23.0 mm hr^{-1}, respectively.

The data fits a curve

$N(D) = N_0 \exp(-\Lambda D)$ $\quad \Lambda = 4.1R^{-0.21}$

$N_0 = 8 \times 10^{-3}\,\text{cm}^{-3}\,\text{mm}^{-1}$

where R is the rain-rate.

Rainfall from tropical maritime air mass

A computed drop size distribution by Srivastova (1971) assumed that drop size was determined by coalescent growth and spontaneous break-up and showed that the final distribution was independant of the initial distribution state but depended on the initial liquid water content.

Fig. 8.2

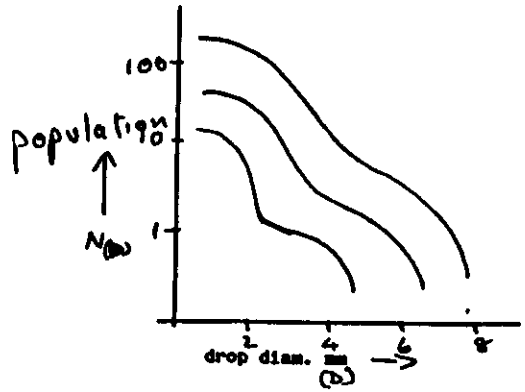

From Doviak

Rain rate and drop size are connected by the terminal velocity of the drops in still air and complicated by vertical air motion. Observed terminal velocities are shown below.

Fig. 8.3

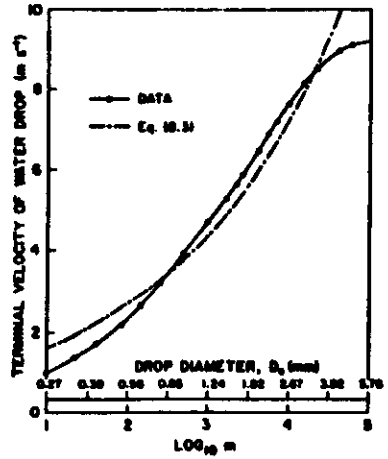

Terminal velocity (solid line) of distilled water droplets in stagnant air at 76-cm-Hg pressure, 20° Centigrade, and 50% relative humidity, as function of the mass m (in micrograms) or the equivalent spherical diameter D_e. (Data from Gunn and Kinzer, 1949.)

Over most of the range the velocity can be adequately described by

$V_t = 386\ D^{0.67}$ where D is the drop diameter.

The number of drops falling through unit horizontal area in time δt of size a to $a + \delta a$

$= N(a)\ V_t(a)\ \delta a\ \delta t$

and the mass of each drop is $\frac{1}{6}\pi\rho_w a^3$

∴ the rain rate in terms of mass per unit area per unit time

$$= \int_0^\infty V_a N_a m_a da$$

$$= \frac{\rho_w \pi}{6} \int_0^\infty a^3 N_a V_a\, da$$

or as a depth of water

$$= \frac{\pi}{6} \int_0^\infty a^3 N_a V_a\, da$$

Substituting for Na, Va and integrate w.r.t. a gives

$$R = \frac{\pi N_0}{\Lambda^4}\left[9.65 - \frac{10.3}{1+\frac{600}{\Lambda^4}}\right] \text{ m s}^{-1}$$

Figure 9.4 shows the relative contribution of different drop sizes to the rainfall rate for a model size distribution and spherical drops falling in still air.

Fig. 8.4

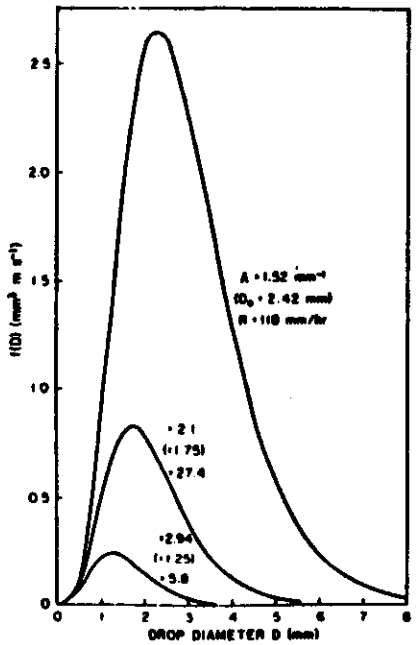

The integrand of the rainfall rate equation (8.18) showing which drops contribute most, assuming an exponential drop size distribution for three different rainfall rates. The rainfall rate integrand is $(\pi N_0/6)f(D) = 10^{-3} f(D) = (9.65 - 10.3e^{-0.6D}) \times D^3 e^{-4D}$

8.2 The cloud liquid water content

The mass of water in drops from size a to $a + \delta a$ is δM

$= \pi/6\, a^3 \rho_w N_a \delta a$

so the cloud water density (M) is

$$M = \int \delta M = \frac{\pi\rho_w}{6}\int_0^\infty a^3 N_a\, da$$

if $N(a) \approx N_0 \exp(-\Lambda a)$

$$M = \frac{\pi\rho_w}{6} N_0 \int_0^\infty [a^3 \exp(-\Lambda a)]\, da$$

$$= \frac{\pi\rho_w N_0}{6}\left(\frac{3!}{\Lambda^4}\right) = \frac{\pi\rho_w N_0}{\Lambda^4}$$

The reflectivity factor is proportional to a^6 the larger drops make the major contribution to the reflectivity factor (Z). For spherical drops

$$Z = \int_0^\infty N_a a^6\ a$$

Figure 9.5 shows the contribution of the different drop sizes to the radar reflectivity. D_0 is the diameter of drops below which half the liquid water content of the cloud is contained.

Fig. 8.5

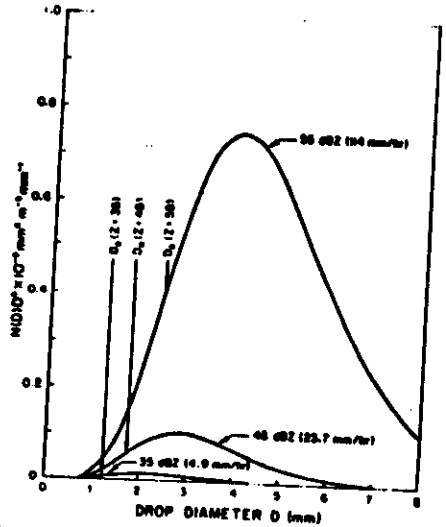

Reflectivity integrand $D^6N(D)$ versus drop diameter for three echo intensities (35, 45, and 55 dBZ). $R = (4\pi/3)(3.67)^{3.76}$ mm hr^{-1}; $N_t = N_0 = 10^4$ m^{-3} mm^{-1}, and D_0 (mm) is the median volume drop diameter

The above results are interesting and, if we could determine the actual drop size distribution in a cloud it is probable that the rainfall rate could be determined from consideration of fall rate and the distortion of the drops. However, the simplest representation of drop size distribution involves two parameters and it is clear that a single measurement of reflectivity cannot provide both parameters. We must therefore resort to empirical relationships if we use a simple calibrated radar or we must obtain additional information by using more sophisticated radar.

Empirical relationships abound. Using the Marshal-Palmer data for rain from stratoform cloud gives

$$Z = 200\,R^{1.6}$$

Different cloud types give rise to different relationships.

e.g. orographic cloud, $Z = 31R^{1.71}$

cumulonimbus cloud, $Z = 486R^{1.37}$

and see Battan for about seventy others!

8.3 Rainfall measurement using dual parameter methods

The fundamental problem with the rainfall rate methods we have discussed so far is that we are trying to measure two unknowns from one data point; the liquid water content and the drop size distribution. If we can obtain two data points we may do better. Hence the development of dual parameter methods for radar rainfall estimation. There are three different possibilities:

a) dual wavelength radars which take account of the different back scattering cross sections of the same drop size distribution at the two wavelengths. The second wavelength is chosen to fall into the Mie scattering region for the larger drops. A difficulty with this technique is that the lower wavelength suffers from attenuation in heavy rain.

b) Reflectivity and attenuation of dual wavelength. Both the attenuation coefficient K and the reflectivity factor Z can be related to Λ and No so the drop size distribution can be determined. This is an interesting research tool but offers little promise as an operational system.

c) Dual polarization of the radar beam and separate measurements of the energy of the reflected signals gives horizontal and vertical reflectivity factors which can again be related to drop size distributions.

9 - SOME OTHER APPLICATIONS OF RADAR

There are many examples of the use of radar in cloud physics and turbulence research. In this section two examples of research with radar are given. They are chosen because of the interesting novel techniques which are applied.

9.1 Radar wind finding in convective storms

Wind fields in clouds are very difficult to determine unless some components of the cloud itself can be used as tracers. Various methods, using two or more doppler radars, have been devised to investigate circulation patterns in storms. One using the "COPLAN" technique is given below.

Two doppler radars on a base line fifty to one hundred kilometers long are used to view the same section of a storm simultaneously and the velocity of the raindrops towards each radar is determined from the doppler shift.

The geometry is illustrated below

Fig. 9.1

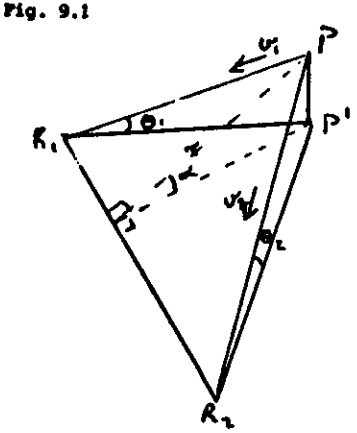

R_1, R_2 radars

P section of cloud being observed

P^1 plan position of P

θ_1, θ_2 elevations of P from R_1 R_2

1, 2 doppler velocities towards R_1 R_2

r the radial distance from P to R_1 R_2 making α to the horizontal

The doppler velocities V_1, V_2 contain a component from the fall speed of the drops. This may be deduced from empirical relationships between Z and the terminal velocity. One such after Atlas et al (1973) is

$$w = 2.65 Z^{0.114} (\rho_0/\rho)^{0.4} \text{ m s}^{-1} \text{ where}$$

w is the population mean terminal velocity and ρ is air density. The Doppler velocities are adjusted to v_1', v_2' where $v_1' = v + w\sin\theta$

From v_1', v_2' two components of the air velocity at P in the plane r, R_1 R_2. For ease of computation the components along and perpendicular to r are used. A series of wind fields are measured in planes containing R_1 R_2. The equation of continuity in a cylindrical co-ordinate system is then used to establish the three dimensional wind field which is then transformed to more conventionall horizontal and vertical co-ordinates. Boundary conditions are zero vertical component at the tropopause and ground surface.

The result of a storm study by Brandes and Johnson* using these methods is illustrated in Figure 9.2

* Reported by Doviak and Zrnic (1984), Doppler Radar and Weather Observations, Academic Press.

Figure 9.2. (a) Contours of reflectivity factor (in dBZ) and the storm relative wind field in a horizontal cross section at 2 km above ground level and (c) a vertical cross section of a tornadic thunderstorm on 2 May 1979, at 16:58 C.S.T. Winds are in the coordinate system moving with the storm. Storm motion speed and direction are shown. Line AB in (a) is the location of the vertical cross section. Distances are from a radar at Roman Nose State Park, Oklahoma (Alberty et al., 1979). The star pinpoints the tornado location in (a). The arrow of indicated velocity at the top right of each plot gives the speed which is proportional to the arrow's length. (From E. Brandes and B. Johnson, NSSL, personal communication.)

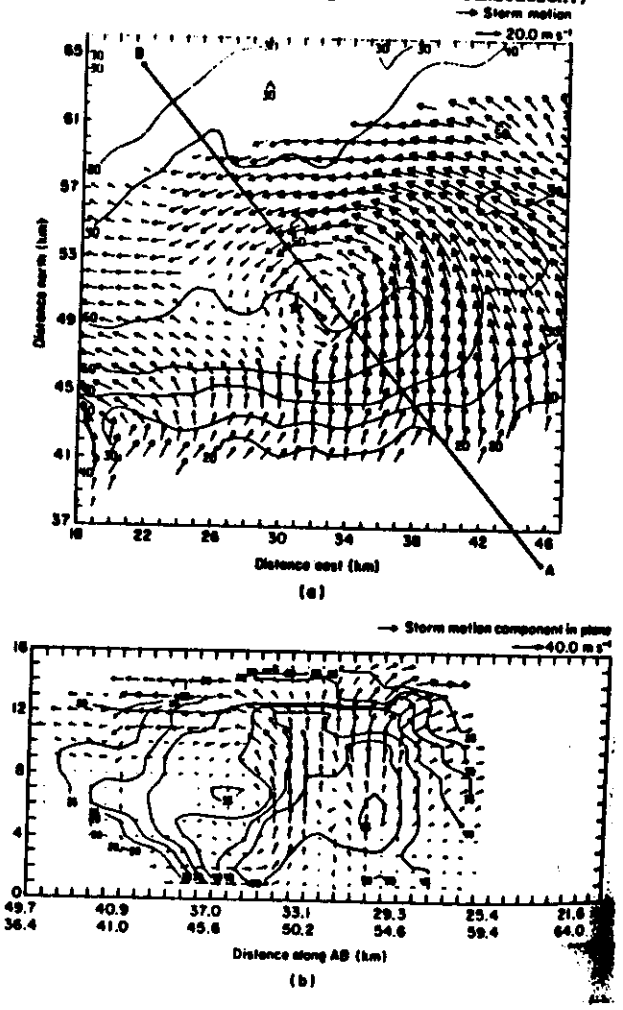

9.2. Radar on satellites

Two problems of satellite borne radar arise from the large distances between the radar and the target. The maximum resolution ($\frac{1.22\lambda}{D}$) means that for a satellite even with a ten metre antenna the ground resolution would be of the order of 10 km for a satellite orbitting at 1000 km and several hundred kilometers for a geostationary satellite. The second difficulty is that of the return power available. With an orbitting satellite the received power is only about 10^{-23} of the transmitted power which is itself much lower than the power transmitted from ground based radar.

Interesting solutions to these difficulties were found on the Synthetic Aperture Radar (SAR).

This radar viewed the earth's surface obliquely at right angles to the direction of travel of the satellite.

Fig. 9.3

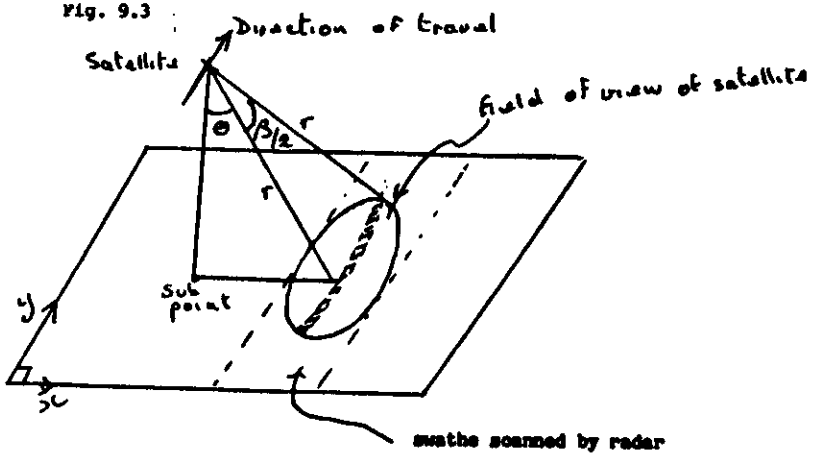

Resolution in the x direction depends on and on the pulse length, and equals ($\frac{\text{pulse length}}{2\cos\theta}$). In the y direction the resolution is $r \sin\beta$

For many purposes neither the x nor the y resolution as described above are adequate.

When a pulse is transmitted and received its power/time curve may resemble

Fig. 9.4

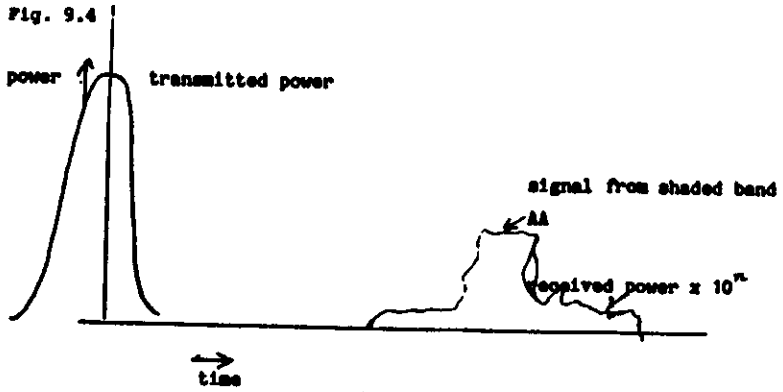

In the SAR both the received power and the x direction resolution are increased by coding the pulse signal by changing its frequency slightly throughout the duration of the pulse.

Fig. 9.5

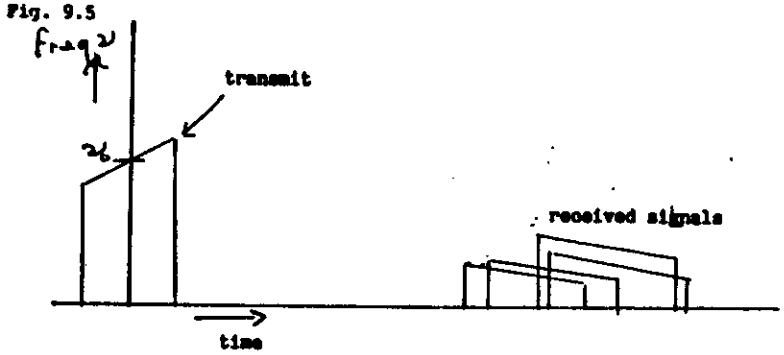

The received signal is then delayed according to its frequency so the whole pulse is compressed after reception, thus increasing power and resolution. This technique is known as the CHIRP.

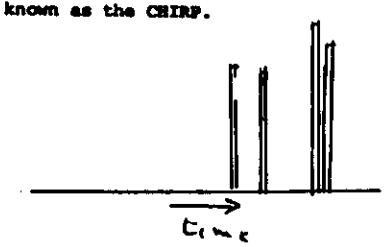

The synthetic aperture method increases the y resolution. The principle is that if a series of identical pulses and echoes are emitted and received by a moving antenna it is possible to recombine the received data as though all the pulses had been emitted simultaneously by a large antenna. The limit of the principle is that any surface point must receive at least two pulses. Hence we have the paradox that the smaller the actual antenna the larger in principle is the resolving power of the synthetic aperture. In fact power considerations giver a lower limit to the antenna size. The higher the pulse repetition frequency (P.R.F.) the more pulses will give information on any one point but the P.R.F. must not be so high that back scatter from two sources could be confused.

A simple analysis of the geometry of the SAR principle is given below.

Fig. 9.6

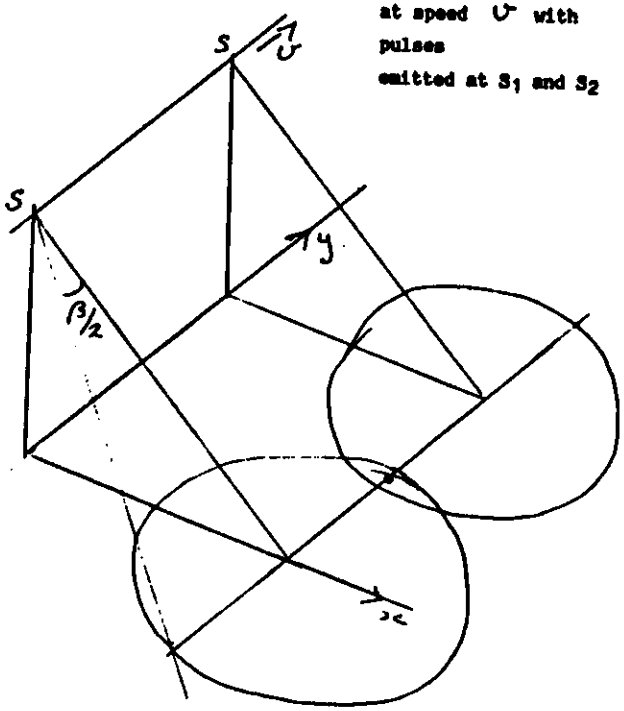

Satellite moving in direction y at speed v with pulses emitted at S_1 and S_2

The size of the synthetic aperture (A_s) may be considered to be the size of the "footprint" in the y direction = $r\beta$

with $\beta = \frac{1.22\lambda}{A_r}$ where Ar is the effective aperture of the actual antenna

So $A_s = \frac{1.22 r \lambda}{A_r}$

and the angular resolution β_s of the synthetic aperature is given by

$$\beta_s = \frac{1.22 \lambda A_r}{1.22 r \lambda} = \frac{A_r}{r}$$

and the linear resolution is A_r.

This is perhaps more easily seen if one considers that the only unique information about the position of a point in the y direction is its doppler shift. The maimum doppler shift is given by

$$\Delta\nu = \nu_0 v\beta/c$$

and for two close points the maximum difference in frequencies of the return signal is given by

$$\Delta F = \nu_0 \frac{v}{c} \frac{\Delta p}{r}$$

where Δp is the y separation of the points

if Δp is the minimum resolvable distance the angular resolution is

$$\Delta p = \frac{r \Delta F c}{\nu_0 v}$$

$$= r \frac{\Delta F \lambda_0}{v}$$

$$= \frac{T \Delta F \lambda_0}{r\beta}$$

$$\propto T \Delta F A_r$$

where T is the time during which a point remains in view of the satellite

but the minimum resolvable frequency is $1/T$ so the linear resolution is Ar. The pulse repetition frequency limits are that a point must remain

in view for more than two pulses

i.e. min P.R.F. $> \frac{v}{A_s}$

Also for signals to be unambiguous the P.R.F. $< \frac{c}{2r}$